Earth-science Reviews
February 2016, Volume 153 Pages 192-211
https://doi.org/10.1016/j.earscirev.2015.11.002
https://archimer.ifremer.fr/doc/00421/53269/

Time-integrated 3D approach of late Quaternary sediment-depocenter migration in the Tagus depositional system: From river valley to abyssal plain

Vis Geert-Jan [1,*], Kasse Cornelis [2], Kroon Dick [3], Vandenberghe Jef [2], Jung Simon [3], Lebreiro Susana M. [4], Rodrigues Teresa [5]

[1] Geol Survey Netherlands, TNO, POB 80015, NL-3508 TA Utrecht, Netherlands.
[2] Vrije Univ Amsterdam, Fac Earth & Life Sci, Dept Earth Sci, De Boelelaan 1085, NL-1081 HV Amsterdam, Netherlands.
[3] Univ Edinburgh, Sch Geo Sci, Grant Inst, Kings Bldg,West Mains Rd, Edinburgh EH9 3JW, Midlothian, Scotland.
[4] Spanish Geol & Min Inst, Dept Res Geol Resources, C Rios Rosas 23, Madrid 28003, Spain.
[5] DivGM, Portuguese Inst Ocean & Atmosphere, Rua Alfredo Magalhaes Ramalho 6, P-1449006 Lisbon, Portugal.

* Corresponding author : Geert-Jan Vis

Abstract :

Quantification of sediment volumes in continental to deep ocean basins is key to understanding processes of sediment distribution in source-to-sink depositional systems. Using our own and published data we present the first quantification of sediment-volume changes in basins along the course of a major southwest European river during the deglaciation. The salient points of this quantitative record in the Tagus and equivalent North Atlantic basins show crucial roles for sea level, climate and land-use in the distribution of sediments. The bypass of sediments starved the Tagus basins, and subsequently sedimentation mainly occurred on the Tagus Abyssal Plain during the sea-level lowstand of the Last Glacial Maximum. The main sediment depocenter rapidly shifted via the continental shelf to the Lower Tagus Valley during sea-level rise in the deglaciation period. Finally, the main sediment depocenter shifted further landward into the Lower Tagus Valley during sea-level high stand in the Holocene. During the high-stand phase (last 7 ky), sediment flux increased up to 2.5 times, due to climate and land-use changes. The average catchment denudation rate during the last 12 ky (0.04-0.1 mm/y) is in agreement with those of other European catchments. Our study clearly demonstrates the added value of detailed knowledge of 3D depocenter distribution, size and chronology. This allowed us to identify an increased sediment flux during the last 7 ky, which was not identified using local observations from boreholes alone. The uniqueness of the Tagus depositional system lies in the combination of a large accommodation space in the bedrock-confined Lower Tagus Valley, the steep lowstand-surface gradient and the narrow continental shelf with canyons indenting the shelf break.

Keywords : Source-to-sink, Sediment budget, Holocene, Incised-valley fill, Sequence stratigraphy, Portugal

1. INTRODUCTION

Studies of sediment-depocentre migration in Quaternary depositional systems provide thorough insights into sea-level, tectonic and climatic controls, but often lack a quantitative approach (Blum and Törnqvist, 2000; Romans and Graham, 2013; Sommerfield and Lee, 2004). Such an approach requires a comprehensive understanding of the source-to-sink system, which consists of areas of erosion, transportation and deposition of sediments. Therefore it comprises investigation of the complete erosional-depositional system from the highest mountain top to the deep sea floor (Sommerfield and Lee, 2004).

A comprehensive overview of studies on sub-modern sediment dispersal in source-to-sink systems is given by Sømme et al. (2009). They rightly state that it is important to understand how geomorphologic elements within a source-to-sink system are related and how sediment is stored and transported at different time scales. In abundant cases, morphology and sedimentology of depositional environments have been described separately. However, little attention has been given to interactions within (and also between) entire source-to-sink systems. A reason for this may lie in the subdivision of disciplines within the earth sciences, which has traditionally led to limited communication across discipline-boundaries.

Nowadays, system-scale interactions as Sømme et al. (2009) refer to, are increasingly studied as a result of new interdisciplinary initiatives. Our work contributes to the call for broader investigation of source-to-sink systems. Many programs have been conducted on recent sedimentary discharge, such as source-to-sink processes of the Eel River sedimentary system in the framework of the STRATAFORM project (e.g. Nittrouer, 1999; Nittrouer et al., 2007; Syvitski and Morehead, 1999; Warrick, 2014). However, limited work focussed beyond the shelf edge (Paull et al., 2014). Other studies of the Californian margin did look across the shelf edge (e.g. Covault et al., 2011; Sommerfield and Lee, 2004), but systems examined were relatively small in catchment size. In Europe a detailed study of the large Rhine River sedimentary system (185,000 km^2) has led to valuable new insights on sediment fluxes during the Holocene (Erkens, 2009), but that study has not taken any marine sediments into account. It is therefore timely to perform a source-to-sink analysis on a sedimentary system with a large catchment, including the marine depocentres. A review of signal propagation in a few systems over different timescales is provided by Romans et al. (this volume).

The main sink for many source-to-sink systems lies at the downstream end: the subaerial and subaqueous delta. In the majority of deltas most sediment is deposited on the continental shelf and slope (Walsh and Nittrouer, 2009; Walsh et al., 2014). This hampers the quantification of sediment volumes, mainly because of the difficulty of determining depocentre size and age and because ocean currents and waves disperse much sediment in along and offshore directions. Ideally, for the quantification of sediment volumes, deposition would be located in an area with maximum control on depocentre extent with minimum sediment export.

The Tagus River sedimentary system approaches this ideal situation. The river is situated in an incised valley, carved out during multiple Quaternary glacial sea-level lowstands. Due to its unique physiography it is well-suited for a quantitative study of sediment production and storage in a source-to-sink system. The river is relatively small on a global scale: the elongated catchment is the tenth largest of Europe and measures about 80,630 km^2. An important attribute is the well-constrained main depocentre which is not located offshore but just inland: the Lower Tagus Valley (Fig. 1). The narrow and deep bedrock-confined Lower Tagus Valley with its steep lowstand-surface gradient is an efficient sediment trap which enables robust volumetric reconstructions. Downstream, the river acts as a point source of sediment on the Iberian passive margin, because large rivers are absent to the north and south of the river mouth. In the marine realm this limits mixing of Tagus sediments with material from other sources. By including the depositional history of the continental shelf and Tagus Abyssal Plain we can obtain a comprehensive understanding of sediment depocentre migration of the Tagus fluvial-marine system since the Last Glacial Maximum. This serves as an example for similar rivers on passive continental margins worldwide.

The overall objective of this work is to evaluate Tagus sediment storage over time and to relate this to source and sink processes. We use a multi-disciplinary and multi-proxy approach to quantify sediment volumes and the timing of deposition. Unlike many studies which often rely on seismic data, our data essentially consist of borehole observations from the terrestrial and marine realm. For the quantification part of this work, the focus lies on the downstream depositional areas, i.e. the fluvial Lower Tagus Valley and the marine continental shelf where the bulk of sediments have accumulated during the last 12 ky (Fig. 2). The main allogenic controls on the fluvial-marine depositional system during this period are relative sea-level change (Vis et al., 2008) and marked aridification of the Iberian Peninsula since the early-mid Holocene (DeMenocal et al., 2000; Fletcher et al., 2007; Magny et al., 2002; Naughton et al., 2007). The marked aridification is shown in regional aeolian dust and pollen records.

We present a new quantitative effort to assess depocentre migration throughout the complete Tagus fluvial-marine sediment dispersal system on the Iberian passive margin during the last 20 ky. We use a time-integrated 3D reconstruction of sediment volumes in the main depocentres during the last 12 ky. This quantitative approach leads to a detailed understanding of depocentre migration and its controls since the Last Glacial Maximum. Using the reconstructed sediment volumes in the depocentres, the amount of deposition per time unit (storage rate) is quantified and the total amount of sediment eroded from the source area (sediment production) in the hinterland is estimated and put in a regional perspective.

2. MATERIALS AND METHODS

2.1 Borehole data and radiocarbon ages

Terrestrial boreholes and cores (385 total) with terrestrial radiocarbon ages (88; Table 1), and detailed reconstructions of valley-fill configuration (Fig. 3) and paleogeography form the basis for the definition of terrestrial depocentre size and timing of deposition (Azevêdo et al., 2006; Brisa, 2005; De Mendonça, 1933; Ineti, 2007; Lusoponte, 1995; Ramos et al., 2002; Ramos Pereira et al., 2002; Van der Schriek et al., 2007; Van Leeuwaarden and Janssen, 1985; Vis et al., 2008). For the marine portion, we used a compilation of 11 cores and 39 radiocarbon ages (Table 1). In particular, two sedimentologically analysed and dated cores, one recovered from the Tagus shelf (D13882) (Weaver, 2003) and one from the landward limit of the Tagus Abyssal Plain (MD03-2698) (Lebreiro et al., 2009). The marine radiocarbon ages were calibrated using the CALIB v5.0 program (Stuiver and Reimer, 1993; Stuiver et al., 2005) and the Marine04 age calibration data (Hughen et al., 2004). The marine calibration incorporated a time-dependent global ocean reservoir correction of about 400 years. Abrantes et al. (2005) proved that this is a good estimate for marine material off Portugal for the last ~110 years; however, older dated material may have been affected by different conditions. For that reason, and to correct for local variations, the difference in reservoir age of the study area and the global ocean was determined ($\Delta R = 262 \pm 164$ y) using the marine reservoir correction database of Stuiver and Braziunas (1993). All mentioned radiocarbon dates are expressed as calibrated calendar ages BP.

2.2 Sediment properties

Grain size was measured using a Fritsch A22 Laser Particle Sizer following the methods described by Konert & Vandenberghe (1997). This included a correction for the measured clay fraction, for everything with a grain size smaller than 8 µm. Microscopic analyses showed that the samples from the marine cores contained little opal, and it was not removed. Grain-size samples of core D13882 (94 total) were taken every 5 cm in the upper 4 m and every 20 cm in the rest of the core. Grain-size samples in core MD03-2698 (40) were also taken at 20 cm intervals, avoiding turbiditic layers. For the identification of these layers, measurements on an X-Ray Fluorescence (XRF) AVAATECH core-scanner at BCR-Bremen were used (Lebreiro et al., 2009). Descriptions and photos of the core are provided in the supplementary material of that paper. The turbidites are very fine (generally mm-thick, occasionally up to 4 cm thick), dark in colour, and have sharp basal contacts. These were identified by particular element peaks in the XRF (e.g., outstanding concentrations of Fe, K, Ti, which were considered typical of continentally derived sediments/turbidites). From terrestrial core VAL (Fig. 4), grain-size samples were taken every 50 cm.

Pollen samples were prepared according to Faegri & Iversen (1975); clastic material was removed using a sodium polytungstate heavy liquid separation. Pollen concentrations were calculated based on added *Lycopodium* marker spore tablets (Stockmarr, 1971). Pollen concentration was calculated based on all pollen and spores in a sample, excluding *Pinus* pollen. The heavy mineral composition of 11 sand samples (~100 cm^3 each) was determined for grains in the fraction 53-420 μm and based on a minimum count of 100 transparent grains per sample. For further details see Busschers et al. (2007).

2.3 Quantifying sediment volume

Sediment volumes for the periods 12-7 ka and 7-0 ka were quantified using 3D spatial models generated in Schlumberger Petrel 2013 software (Fig. 5). 3D bounding surfaces were modelled using convergent (geo-statistical) interpolation. The upper bounding surface of the model is represented by present-day topography and bathymetry. Onshore, this surface consists of hole-filled seamless SRTM data with a 90x90 m resolution (Jarvis et al., 2006). For the Tagus estuary, bathymetric maps (numbers: 26304, 26305, 26306 and 26307) were used (Instituto-Hidrográfico-Portugal, 2008). For the seafloor bathymetry, bathymetric map 24204 (Instituto-Hidrográfico-Portugal, 2008) and bathymetry by IPMA-DivGM (2013) were employed. The lower (12 ka) and middle (7 ka, only used in the Lower Tagus Valley) bounding surfaces were created based on their sedimentological identification in boreholes. The location and extent of upstream buried terraces were added to the model based on boreholes and palaeogeographic reconstructions (Vis et al., 2008). For volumetric modelling, every 90x90 m grid cell was multiplied by the height of the sediment column between the upper and lower bounding surface.

2.4 Volume to mass conversion using dry bulk density

Conversion of sediment volume to mass requires dry bulk density values (ρ = ratio of mass of mineral grains to total volume). Dry bulk density is mainly influenced by grain-size distribution (lithology or facies), compaction and the organic matter/carbonate content of the sediment. By reducing porosity, sediment compaction increases bulk density. Compaction is mainly controlled by the spatial distribution of lithology, the overlying load, the compaction response time of sediment layers and groundwater fluctuations (Kooi and de Vries, 1998; Van

Asselen et al., 2009). Generally, sand and gravel can be minimally compacted; clay can be compacted to a moderate degree, and peat is highly compressible (Allen, 1999).

The deposits in the Lower Tagus Valley mainly contain clay, silt and sand; the volume of peat is negligible. In the narrow northern part of the valley, the fluvial deposits have been or are partly exposed to low groundwater levels, leading to denser, more compacted sediments. Nonetheless, due to the limited width (3-6 km) and thickness (on average 5-8 m), their volume is relatively small. In the large low-lying southern part of the valley, the tidal and prodelta sediments were deposited mainly sub-aquatically. At present the groundwater is within a few meters of the surface, which has limited compaction due to dewatering. Cone penetration tests (CPT) in the thick sediment layers in this area indicate soft to very soft deposits, with limited to no compaction. The CPT values from the shallow marine and tidal muds do not exceed 4 Mpa and do not increase with depth within those facies, indicating limited or no compaction. The tidal sands have average CPT values around 18 Mpa. In contrast, CPT values in the sand and gravel-rich fluvial lowstand deposits generally do not drop below 35 Mpa (Brisa, 2005; Lusoponte, 1995). On the continental shelf, some sediment compaction may have taken place, especially in the thick subaqueous delta. However, this delta is assumed to contain much sand which hardly compacts (Mougenot, 1985). Based on the above, we assume the effect of compaction on the calculated sediment mass to be limited.

Various studies demonstrate the great variability of dry bulk density across a delta resulting from alluvial architecture and facies (e.g. Erkens and Cohen, 2009; Shi et al., 2003). As the deposits which accumulated in the Lower Tagus Valley in the period 12-7 ka mainly consist of fine-grained tidal marsh and marine deposits, we used a sand to clay loam to silty clay ratio of 0.1:0.45:0.45. Using a bulk density of 1.75 t/m^3 for sand, 1.4 t/m^3 for clay loam and 1.2 t/m^3 for silty clay (Erkens and Cohen, 2009) resulted in a weighted average density of 1.35 t/m^3. This ratio was chosen to account for the facies present in the valley fill. During the period 7-0 ka, more sand-rich deposits (river channels, tidal sands) accumulated in the Lower Tagus Valley, with an estimated sand to clay loam to silty clay ratio of 0.4:0.3:0.3. and weighted-average dry bulk density of 1.48 t/m^3. For the heterogeneous proximal subaqueous delta a dry bulk density of 1.50 t/m^3 was used (Goodbred and Kuehl, 2000), and for the prodelta the dry bulk density for mud was assumed (1.15 t/m^3).

The amount of carbonate and organic matter in the Lower Tagus Valley sediments ranges between 0 and 5% (by weight) for each constituent. Because no detailed data on the distribution of carbonate and organic matter are available and because the dry bulk density of organic matter is very low, no correction for these constituents has been made.

3. DEPOCENTRES AND SEDIMENT VOLUMES

3.1 Land: Lower Tagus Valley depocentre

3.1.1 Lower Tagus Valley depocentre configuration

The terrestrial depocentre consists of a ~100-km-long, up to 10-km-wide and up to 80-m-thick sediment body in the Lower Tagus Valley (Fig. 3). This confined valley is bordered by Mesozoic and Cenozoic deposits in the west and Quaternary terraces in the east. The valley has been successively incised during Quaternary glacial sea-level lowstands, of which the latest incision created the accommodation space for the thick Holocene valley fill (Fig. 4a). The Tagus River leaves the valley through a 2-km-wide bedrock-restricted gorge south of Lisbon.

The palaeogeography of the Lower Tagus Valley forms the basis for the 3D quantification of sediment volume. It is based on the extensive study of spatial and temporal changes of sedimentary environments in nine cross sections through the valley fill (Vis et al., 2008). Environments were identified by means of lithological and sedimentological data, combined with floral (pollen, terrestrial botanical macro remains, diatoms) and faunal (shells, foraminifera, dinoflagellates) indicators (Vis et al., 2008; Vis et al., 2015). The timing is provided by radiocarbon ages (Table 1). Sea-level reconstructions by Hanebuth et al. (2000) and Vis et al. (2008) were used to define palaeo-water depth and coastline position.

The upper bounding surface is based on SRTM-derived elevation, which was cross-validated using topographic maps and showed very limited elevation offsets on the floodplain (<2 m). For the subaquatic part we used the detailed bathymetric maps, making it a robust bounding surface. The lower (12 ka) and middle (7 ka) bounding surfaces, however, are less robust since they are based on a dataset of boreholes and palaeogeographic interpretations. The lower bounding surface corresponds with the top of the Pleistocene fluvial lowstand deposits; its position is inferred from 283 boreholes and palaeogeographic interpretation (Vis et al., 2008). The middle bounding surface corresponds with the maximum flooding surface, which dates to 7 ka based on 12 radiocarbon ages (Vis and Kasse, 2009). In the narrow and shallow upstream section of the Lower Tagus Valley, the position of this surface has been interpreted using sedimentology in 30 boreholes. In the wider and deeper valley further downstream, the middle bounding surface was noted in 95 boreholes. Around 7 ka the wide tidal basin in the south had a relatively flat bottom, permitting relatively simple interpolation of the maximum flooding surface there.

3.1.2 Lower Tagus Valley depocentre volume

The sediment volume which accumulated in the Lower Tagus Valley between the lowstand surface of ~12 ka and the upper bounding surface measures ~20.2 km^3 (Fig. 6a, Table 2). The aforementioned maximum flooding surface (~7 ka) was used to calculate differences in sediment accumulation between the retrograding and prograding systems. Our results show that about 13.9 km^3 of sediment accumulated between the maximum flooding surface and the present-day topography. Subtracting this value from the total Lower Tagus Valley sediment volume (20.2 km^3) reveals that the total volume deposited between 12 and 7 ka is ~6.4 km^3.

3.2 Continental shelf: subaqueous delta depocentre

3.2.1 Continental-shelf depocentre configuration

The marine depocentre consists of the subaqueous delta. For the purpose of our study we divided the subaqueous delta in a thick proximal part (morphologically known as subtidal platform and delta front) and the prodelta (Figs 1c, 2 and 5). The proximal subaqueous delta measures about 15x15 km with an estimated sediment thickness of 60-70 m. This thickness estimate is based on extrapolation of the relatively flat continental shelf surface from alongside the subaqueous delta to underneath the delta. Unfortunately no borehole or seismic data were available, which would allow more precise thickness estimates. The proximal subaqueous delta covers the underlying lowstand fluvial valley, which has been filled with sediment during sea-level rise (Mougenot, 1985). To estimate the relatively minor volume of this valley-fill, we used bathymetry based on the palaeogeographic reconstruction by Vis et al. (2008). The complete proximal subaqueous-delta volume was calculated using the bathymetry from the palaeogeographic reconstruction of 7 ka as the basal surface and by taking the present-day bathymetry as the upper surface.

The prodelta (Figs. 6b and 7a) is considered to be an outward thinning, low-gradient deposit (cf. Jouanneau et al., 1998). However, poorly constrained morphological boundaries and diffuse sediment dispersal in the marine realm complicate calculation of shelf sediment volumes. Despite the narrow shelf, most sediment has probably remained on the shelf, constraining the post-7 ka deposition of fluvial-derived sediment (Jouanneau et al., 1998). Also see the discussion in section 3.2.2.

The area of the prodelta measures about 550 km^2 (Alt-Epping et al., 2009) and its extent is based on seafloor samples and box and gravity cores (Alt-Epping et al., 2007; Jouanneau et al., 1998). To estimate the volume of this area, we adopted a similar approach as for the proximal delta. The lower bounding surface was extrapolated underneath the mudbelt as a flat surface consistent with the surrounding continental shelf. The thickness of this relatively thin and flat sediment body is relatively well-constrained due to the 10 boreholes penetrating it (Fig. 1c).

3.2.2 Continental-shelf depocentre volume

The volume of sediment that was deposited on the Tagus shelf between 12 and 7 ka appears to be relatively small as illustrated by the thin sequence in core D13882 (Fig. 7a). Core data indicate low sedimentation rates on the shelf between 12 and 7 ka due to the rapid post-glacial transgression and efficient sediment trapping in the Lower Tagus Valley (Fig. 4). Therefore the 12-7 ka shelf sediment volume is assumed to be limited. Furthermore, there are no data to constrain location, extent and timing of deposition of a pre-7 ka sediment body, so volumetric calculations of sediment were made for the period after 7 ka. This is the period during which reconstructions indicate that the subaqueous delta built up (Fig. 6b) (Mougenot, 1985; Vis et al., 2008).

Our calculations show that the proximal subaqueous delta contains ~5.5 km^3 of sediment and the prodelta ~0.7 km^3 (Fig. 6b, Table 2). The relatively small volume of prodelta sediments suggests that exclusion of the pre-7 ka shelf deposits has a minor impact on the sediment budget, although it may cause a limited underestimate of the total 12-7 ka sediment volume.

To check the validity of the calculated volume of post-7 ka prodelta mud, we divided the volume by the surface of 550 km^2. This resulted in an average thickness of 1.2 m. Because the cores we used encountered 6-7 m of post-7 ka sediment, the average thickness seems conservative. However, these cores were targeted at the thickest part of the prodelta. Large peripheral parts are expected to be relatively thin, implying that the average thickness of 1.2 m is probably realistic.

A portion of the fluvial sediment transported to the Tagus marine realm has possibly moved along-shore or past the shelf break during the last 12 ky. This portion was not included in the marine volumetric calculations. A bottom nepheloid layer is known to transport sediment to the head of the Lisbon canyon (Fig. 1c), but most of it fails to reach the Tagus Abyssal Plain (Jouanneau et al., 1998). This is corroborated by reduced concentrations of suspended sediment into the water column and low depositional fluxes in sediment traps and multicores in the Lisbon-Setúbal canyon (Richter et al., 2009). More recently two studies using present-day measurements of suspended particulate matter and using cored sequences, concluded that the Lisbon and Cascais canyons have been virtually inactive with respect to down-canyon sediment transport since ~8 ka (De Stigter et al., 2011; Masson et al., 2011). Some sediment may accumulate in the head of the canyon, but that volume is considered to be small relative to the volumes considered. However, Lastras et al. (2009) have identified sediment bedforms in the canyons, which suggests the canyons may act as efficient conduits for sediment from the continental shelf to the abyssal plain during high-energy events. Nonetheless, we estimate the volume of sediment leaving the shelf depocentre during the studied time interval as negligible when compared to the total deposited sediment volume. Cores retrieved from sediments on terraces in the Lisbon and Cascais canyons indeed show only hemipelagic sedimentation with rare turbidite activity during the last ~8 ky (Masson et al., 2011).

In general, the accuracy of the offshore palaeogeographical reconstruction and sediment volume are limited, because the internal structure and exact timing of deposition of the buried canyon and subaqueous delta are unknown. Furthermore, the subaqueous delta may be partially composed of sediments with a marine source, which would reduce the volume of terrestrially sourced sediment. But, the budget as constructed provides a best-estimate for marine storage.

3.3 Deep sea: Tagus Abyssal Plain depocentre

3.3.1 Tagus Abyssal Plain depocentre configuration

The Tagus Abyssal Plain depocentre (-4500 m msl; Figs. 1 and 8a) consists of turbidite deposits alternating with pelagic beds (Alves et al., 2003; Lebreiro et al., 2009; Lebreiro, 1995; Masson et al., 2011). Most turbidites are the result of Tagus sediments which bypassed the continental shelf and slope during low relative sea-level. They were most likely generated at the heads of the Cascais and Lisbon-Setúbal canyons after collapse of an accumulated sediment body. The Tagus Abyssal Plain is very large (~46,000 km^2), and it is unclear which part of it receives sediment from the Tagus River. The thickness of the Tagus-sourced deposits is likely to vary across the plain, but the limited availability of radiocarbon-dated cores hampers the compilation of age-thickness distribution maps.

3.3.2 Tagus Abyssal Plain depocentre volume

For the Tagus system, the estimated volume of turbidites deposited on the Tagus Abyssal Plain is ~3500 km^3 per million years (Weaver et al., 2000). Most of this was probably deposited during glacials when sediment was transferred past the shelf to the deep sea. This assumption is supported by observations from cores recovered about 200 km west of our MD03-2698 core on the Tagus Abyssal Plain (Fig. 1 in Masson et al., 2011). Core D11951 shows that hemipelagic sedimentation decreased by a factor of two between 18 and 14 ka (Masson et al., 2011), which is around the same time that turbidite deposition in core MD03-2698 ended (Fig. 8). About five turbidites have been recorded in sediments from the last 12 ky in the distal Tagus Abyssal Plain. These are interpreted to reflect seismic events, which triggered landslides in the canyons, on the continental slope and from the levee between the Setúbal and Cascais canyons (Masson et al., 2011).

Hemipelagic and turbidite deposition have taken place on the Tagus Abyssal Plain since the deglaciation, but the bulk of turbidite-generated sediment volume during the last 12 ky appears to be from landslide-sourced sediment which is not considered part of the current sediment budgeting exercise. The hemipelagic component is small and partly not siliciclastic due to a high carbonate content (see section 4.1), and the source of the siliciclastic component is unclear. It is difficult to reliably estimate the extent of the Tagus Abyssal Plain depocentre and configuration for sediment-volume calculations. For the abovementioned reasons, we have assumed negligible sediment storage in the area after 12 ka and not examined the budget prior to 12 ka, because of potential and unconstrained storage in deep water.

4. DISCUSSION

4.1 Depocentre migration

During the Last Glacial Maximum, sedimentation in the Lower Tagus Valley and on the exposed shelf was limited. The shelf break lies around -200 m relative to present-day sea level (Fig. 1). Although lowstand relative sea level remained 30-70 m above the shelf break, fluvial sediments bypassed the shelf via incised valleys directly funnelling into the heads of marine canyons (Fig. 1). The bypass of fluvial sediment to the deep sea resulted in relatively high-frequency turbidite deposition (up to 10 turbidites per 500 y) near the Tagus Abyssal Plain between 20 and 15 ka (Lebreiro et al., 2009). Around 15 ka the deposition of turbidites virtually stopped (Fig. 8a), reflecting the relative sea-level rise after the Last Glacial Maximum (Fig. 9). Simultaneously, the Tagus changed from a braided into a single-channel river due to climate change affecting discharge and increasing the production and load of fine-grained sediment (Vis and Kasse, 2009). Although the deposition of turbidites had virtually stopped, siliciclastic hemipelagic sedimentation on the abyssal plain continued at a relatively high rate until ~12 ka (~1.3 mm/y, Fig. 8d). This high rate reflected a continued strong supply of fluvial-derived sediment to the abyssal plain due to the efficient bypass of sediment through the canyons during low relative sea-level. This is also indicated by the high pollen concentration (Fig. 8c), because pollen grains behave as fine-grained sediment (Chmura and Eisma, 1995). The pollen concentration can be considered a proxy for the ratio of terrestrial to marine sediment input. Pollen were mainly supplied by the Tagus River, because aeolian supply was limited due to a dominance of landward winds (Naughton et al., 2007).

The final stage of rapid abyssal plain deposition from 15-12 ka is assumed to overlap with the beginning of shelf sedimentation on top of lowstand fluvial deposits before ~13 ka (Fig. 7). Around 12 ka the bypass of sediment to the Tagus Abyssal Plain slowed rapidly, resulting in a six-fold decrease in sedimentation rate (from ~1.3 to ~0.2 mm/y; Fig. 8d). Consequently, pollen concentrations in the sediments are five times lower than during the preceding period, and post 12 ka sediments are carbonate-rich (20-40 %) (Lebreiro et al., 2009), implying little siliciclastic sediment transfer to the deep sea during rising and high relative sea level (Fig. 9). Decreased sedimentation rates including strongly reduced turbidites are corroborated by a recent study of canyon and Tagus Abyssal Plain cores (Masson et al., 2011). We interpret this decrease in deposition on the Tagus Abyssal Plain to reflect a landward depocentre shift (Fig. 9). Since 12 ka there was little sedimentation on the abyssal plain and most sedimentation occurred further landward in the system.

Sedimentation on top of the fluvial deposits formerly exposed on the continental shelf started at ~13.5 ka with a high initial sedimentation rate (~2.6 mm/y) during the pre-Holocene period (Fig. 7d). A sandy interval was deposited in the early stage of the Holocene (~10.5-5 ka), coinciding with the maximum flooding surface. This interval resulted from a period when fluvial mud was mainly trapped in the Lower Tagus Valley and mud supply to the shelf was low, limiting deposition and making winnowing by bottom currents more effective relative than in the preceding period (Vis et al., 2010a). The resulting low sedimentation rate on the shelf (~0.3 mm/y; Fig. 7d) is corroborated by a decreased concentration of organic matter and terrestrial plant proxies after the onset of the Holocene (Rodrigues et al., 2010). The low sedimentation rate and low fluvial-derived particle input are also supported by the lowest pollen concentration (Fig. 7c). Around 5.5 ka, the sedimentation rate increased to an average of ~1.2 mm/y due to an enhanced supply of terrestrial material to the shelf, supported by an up to eightfold increase in pollen concentration. This change reflects decreased sediment trapping in the Lower Tagus Valley, and increasing deposition on the shelf.

Rising relative sea level created accommodation space in the Lower Tagus Valley, which caused fluvial aggradation in the valley since ~12 ka in the valley, followed by transgressive tidal and shallow marine sedimentation (Figs. 4 and 9). Increasing sediment volumes were trapped in the Lower Tagus Valley. This resulted in strongly reduced sediment export to the shelf as noted. Until about 7 ka, the depocentre shifted landward where Lower Tagus Valley accommodation space was maximal.

The end of relatively rapid sea-level rise at ~7 ka is marked by the maximum flooding surface, the onset of bayhead-delta progradation in the Lower Tagus Valley, and the build-up of a fluvial sediment wedge (Fig. 6c) (Vis et al., 2008). Around 7 ka, the valley was filled to such an extent (6.5 km^3, Table 2) that gradually sediment export to the ocean increased again (Figure 7d). This shift of the depocentre caused a progressive seaward build-up of the subaqueous delta (Fig. 9). From 7 ka to the present, the Lower Tagus Valley and shelf depocentres accommodated 20.1 km^3 of sediment (Table 2). Since ~2 ka deposition in the fluvial and shelf depocentres increased (Fig. 9). In the Tagus valley grain size coarsened; sedimentation rates tripled; organic matter levels in the sediment decreased, and magnetic susceptibility increased. On the shelf, the grain size of accumulating sediment fined, and sedimentation rates and magnetic susceptibility increased (Vis et al., 2010a). These changes were caused by land-use changes in the Tagus catchment, which overwhelmed the sedimentary signal of possible climatic changes (Vis et al., 2010a).

The large amount of core information available for the Lower Tagus Valley allows for the establishment of the detailed relationship between stratigraphic surfaces and facies architecture—the essence of sequence stratigraphy (Catuneanu et al., 2009). In terms of the incised-valley fill (Fig. 10), the postglacial Tagus depositional system generally resembles many of the systems described around the world (e.g., Blum et al., 2013; Dalrymple et al., 1994; Dalrymple, 2006; Simms et al., 2006; Törnqvist et al., 2006). The uniqueness of the Tagus depositional system lies in the combination of a large accommodation space in the bedrock-confined Lower Tagus Valley, the steep lowstand-surface gradient (~0.60 m/km) and the narrow continental shelf (<30 km) with the Cascais and Lisbon canyons indenting the shelf break (24 and 13 km from river mouth to canyon head respectively; Fig. 1). The steep lowstand-surface gradient is responsible for a large volume of accommodation space in the narrow valley. The marine canyons were probably directly connected to the lowstand river valley (Vis et al., 2008), which efficiently transferred sediment to the abyssal plain during the glacial period, despite a relative sea-level lowstand which remained 30-70 m above the shelf break (Fig. 1, profiles a-a' and b-b'). This direct connection is known from other studies, but the number of observations remains limited (Holbrook and Bhattacharya, 2012; Talling, 1998). Small bay-head deltas possibly built up in the drowned river valleys or canyon heads, but due to the steepness of their floors, the deltas probably collapsed regularly, leading to the observed high-frequency turbidites on the Tagus Abyssal Plain.

Sediment storage in the Lower Tagus Valley caused a reduction of abyssal plain sedimentation on this passive margin. The reduction is much larger than that reported for example for the tectonically active southern California margin, where similar studies were performed (Romans et al., 2009; Sommerfield and Lee, 2004).

4.2 Sediment storage rates

To understand sedimentation in the Tagus depocentres during the periods 12-7 ka and 7-0 ka, we calculated the mean sediment storage rates (Table 2). During the oldest time period, most sediment was deposited in the Lower Tagus Valley because relative sea level shifted the depocentre to that area (Fig. 9). A limited amount of sediment was deposited on the continental shelf. The mean sediment storage rate during this interval was 1.7 x 10^6 t/y (Table 2). The younger interval was characterized by deposition in both the Lower Tagus Valley and on the continental shelf, due to a seaward shift in sedimentation (Fig. 9). The mean sediment storage rate for this interval was 4.2 x 10^6 t/y (Table 2). This is a ~2.5 times increase in the mean rate of sediment storage, when compared to the previous period.

The mean sediment storage rates from the time intervals 12-7 ka and 7-0 ka for the Lower Tagus Valley depocentre *alone* show an increase of ~1.7 times during the latter period (Table 2). The reason for the increase most likely is a strongly increased terrestrial sediment yield. Because some suspended sediment escaped from the system due to coastal and marine currents during both periods (as shown by the presence of clay in the Holocene section of the Tagus Abyssal Plain core), more sediment was likely supplied to the marine realm but it is unaccounted for in this budget.

A cause for the increased sediment yield may be found in a changed climate. During the investigated period the African Humid Period (~11.5-5.5 ka) ended due to gradually decreasing summer insolation, leading to weakening of the African summer monsoon in the Mediterranean and North Africa (DeMenocal et al., 2000; Renssen et al., 2006). On the Iberian Peninsula, this led to regional aridification and a progressively decreasing forest cover, with increased herbaceous vegetation (Carrión et al., 2007; Fletcher et al., 2007). The less dense vegetation likely increased soil erosion, and thus Iberian fluvial sediment yields, leading to floodplain aggradation (Thorndycraft and Benito, 2006; Wolf et al., 2013). The similar timing of the weakening summer monsoon, decreased forest cover, increased sediment yields, and raised mean sediment storage rates of up to ~2.5 times in the Lower Tagus Valley and shelf, imply a causal relationship between the above observations. Besides climate, another driver of the increased mean storage is increased human impact during the last ~2 ky; sedimentation rates are considered to have tripled because of land-use changes (Vis et al., 2010a). Many systems around the world have shown an anthropogenic response as noted in Kuehl et al. (this volume) and Romans et al. (this volume).

4.3 Robustness of sediment volumes and storage rates

Several studies of depositional systems have addressed difficulties in constraining sediment loss beyond the immediate system by, for example, surface plumes or coastal currents (Kuehl et al., this volume; Miller and Kuehl, 2010; Sommerfield and Lee, 2004; Sommerfield et al., 2007; Warrick, 2014). As discussed above, the Tagus depocentres are considered to have a high trapping efficiency, especially the Lower Tagus Valley. This implies that during the last 12 ky limited sediment was exported seaward. We therefore assume the calculated sediment volumes in general to be relatively robust, especially when compared to many other deltaic systems in the world. The input of marine-sourced sediment is limited as well, since heavy mineral analyses of Lower Tagus Valley sands demonstrate a fluvial provenance (Fig. 11).

In the Lower Tagus Valley, the channel belt experienced little lateral migration, and avulsions have not occurred (Vis et al., 2008). Today the system is still aggrading and prograding, so sediment recycling due to lateral channel-belt migration has been limited. The calculated sediment volumes are therefore likely to contain a limited amount of reworked sediment and quite accurately reflect input.

The quantification of accuracy and precision of sediment volumes and sediment storage rates is hampered by the nature of the data, which consist of geologically interpreted data from boreholes. To capture the heterogeneity of the terrestrial realm, boreholes were placed with a variable horizontal spacing (50-1000 m) along cross sections, which themselves were placed at a more or less regular spacing in the Lower Tagus Valley (Fig. 1b). The limited number and spatial distribution of offshore boreholes implies a less robust knowledge of depositional architecture, leading to a reduced accuracy of marine depocentre size and lithology. Besides boreholes, lithological sampling resolution, sedimentological interpretation in terms of facies, and palaeogeography all involve steps in the process which affect accuracy. The construction of timelines, for example, is more robust in distal non-erosive flood basin deposits than in channel or tidal-marine deposits which have less borehole control and potentially greater spatial variability. The main factors affecting both the accuracy and precision of sediment volumes and storage rates are depocentre geometry, lithology, bulk density and dating. Geometry is mainly affected by the reconstructions and interpolations of the bounding surfaces. To test the sensitivity of sediment volume to geometry, we lowered the basement surface in the Lower Tagus Valley by 10% and recalculated the total 12-0 ka sediment volume. The recalculated volume is ~9.5% larger due to that change, and based on this, we estimate the error in geometry of all bounding surfaces to be less than ±10%.

The spatial distribution of lithology and dry bulk density and thus facies is based on many factors discussed above. Dry bulk density measurements for the study area are scarce. An unpublished study related to the construction of a motorway bridge across the large low-lying southern part of the valley reports dry bulk density values for 37 samples (Brisa, 2005). The measurements show no significant increase of dry bulk density with depth (3-35 m) and range between an average of 1.22 g/cm^3 for sandy silty clay and 1.06 g/cm^3 for silty clay. These samples represent shallow marine and tidal muds which were deposited both in the 12-7 ka interval and the 7-0 ka interval. These values are lower than the dry bulk densities we used (Table 2), because our values include more indurated, denser fluvial flood basin deposits in the upstream reach and denser sand-dominated channel belt deposits. The dry bulk densities we used are based on varying sand-mud ratios. In general, the sensitivity of the calculated sediment mass to changes in dry bulk density of ± 0.1 t/m^3, reaches up to ± 9 %. Changing the sand-mud ratio with ± 0.1, results in a ± 0.05 t/m^3 change of the dry bulk density and thus ± 3.5 % in sediment mass. Therefore, dry bulk density is a worthwhile factor to consider when possible.

All ages for this study were obtained using radiocarbon dating of terrestrial and marine organic material, and the accuracy and precision of the ages is determined by the quality of the dated material, the dating method and interpretation of their significance. The measurements have a relatively high accuracy and precision because of the relatively young age of the deposits with respect to the radiocarbon range. Due to the large number of radiocarbon dates, combined with regional geological data, we are confident that the variability in sediment volumes is affected little by the radiocarbon dates, and in sum, the storage amounts are relatively robust.

To better understand the balance between climatic and anthropogenic controls on the increased mean storage rate during the last 7 ky, we calculated two scenarios. In the first scenario, the lower 12-7 ka mean storage rate (1.7×10^6 t/y) was continued until 1 ka. The difference between the total sediment mass present in the depocentres (3.8×10^{10} t) and the mass resulting from 11 ky at 1.7×10^6 t/y (1.9×10^{10} t) was divided by 1 ky, to get the mean storage rate needed to supply the remaining 1 ky of sediment (1.9×10^7 t/y). This leads to an increased mean storage rate for the last 1 ky of ~11 times, which seems unrealistic. The same method was applied for the second scenario, but with the time slices 12-3 ka (1.5×10^6 t/y) and 3-0 ka (7.6×10^6 t/y). This increases the mean storage rate for the last 3 ky ~4 times. This exercise demonstrates that a hypothetical steady mean storage rate between 12-1 ka, followed by an 11-fold increase to 1.9×10^7 t/y for the final 1-0 ka period, exceeds the tripled sedimentation rate as observed in field data for the last 1 ky (Vis et al., 2010a). Also an extended late Holocene period (3-0 ka) with an increased mean storage rate (to 7.6×10^6 t/y), still requires a 4-fold increase of mean storage rate. Therefore, besides anthropogenic causes it is likely that climate-related changes have increased the mean sediment storage rate during the last 7 ky.

In sum, the budget presented is considered robust, although differences in the geometry of the bounding surfaces and different assumptions for the average dry bulk density may have a summed effect of 10-20% on the sediment volumes.

4.4 Estimating Holocene catchment denudation

In many catchments sediment transport measured in river channels is not representative for millennial-scale natural sediment yield due to strongly increased human-induced sediment production during the last centuries. Recently this increase has been counteracted by a load decrease induced by the construction of dams and reservoirs (Vörösmarty et al., 2003). The Tagus River is one of the most reservoir-impacted rivers in the world (Syvitski et al., 2003), and has seen a great increase in sediment flux due to human activities in both on and offshore environments (Vis et al., 2010a). Because of the strong imprint of human activities on the river, the establishment of long-term catchment denudation rates (mm/y) based on multi-centennial sediment volumes will be useful in future discussions on the natural versus human-impacted state of the river.

4.4.1 Sediment load

Catchment denudation is the net effect of weathering, slope processes and fluvial transport and results in a solid (sediment) and solute (dissolved) load in the river leaving the catchment. The solute load for the Tagus River is unknown, and its quantification is beyond the scope of this study. The solid load consists of bedload and suspended load. Estimates of bedload transport show that since the 1950's the construction of dams in the Tagus River has caused a decrease of bedload transport from ~1.2×10^6 m^3/y to ~3.5×10^5 m^3/y, a reduction of 71% (Quintela et al., 1982; Ramos and Reis, 2003). The average suspended load of the river after construction of dams ranges between ~4.0 x 10^5 t/y (Vale and Sundby, 1987) and ~4.5 x 10^5 t/y (Rocha et al., 2005). The reported post-dam bedload volume of ~3.5 x 10^5 m^3/y can be converted to t/y (using a porosity of 20% and grain density of 2.65 t/m^3). This yields ~1.9 x 10^5 t/y of bedload, which is ~30% of the total post-dam solid load (using ~4.5 x 10^5 t/y for suspended load). For comparison, in the Rhine-Meuse delta, bedload represents ~41% of total solid load for the last 9 ky until embankment and dam construction (Erkens and Cohen, 2009).

The abovementioned solid load data are based on measurements from the last 70 years. Therefore they do not reflect the long-term natural situation as it existed before 2 ka or even longer ago. This study provides valuable insight in long-term average sediment load of the Tagus River, under natural and human-influenced conditions, which are needed for estimating catchment denudation.

4.4.2 Sediment delivery ratio

For a source-to-sink comparison, catchment denudation rate can be calculated based on a volume of sediment in a downstream depocentre. For the Tagus depositional system this basically consists of the Lower Tagus Valley depocentre and the shelf depocentre. This is atypical, since many rivers have their main depocentre seaward of the coastline (Walsh et al., 2014). When converting the sediment volume in the depocentre to a denudation rate, we recognize that the deposited volume must be smaller than the originally eroded volume in the catchment. This is because much sediment is trapped in footslopes, concavities, alluvial plains and other sinks (De Vente et al., 2007). To correct for that discrepancy we use the sediment delivery ratio, which is the proportion of sediment mobilized on catchment slopes which is delivered to the coastal zone (Walling, 1983).

The sediment delivery ratio is difficult to establish (see discussion in De Vente et al., 2007; Lu et al., 2005; Walling, 1983). Many estimates have been published from various regions, timescales and catchment sizes (Table 3). Despite the large spread in sediment delivery ratios, a very general trend is that larger catchments on average have lower sediment delivery ratios. A comparison of sediment delivery ratios of various catchments in similar climates indicates that the Tagus catchment should have a ratio of 20-45% (Fig. 1 in Ferro and Minacapilli, 1995).

The period considered in this study follows a glacial period during which prolonged deep incision and erosion of the Tagus catchment took place and excavated much catchment-stored sediment. During the following 12 ky up to the present day, many storage areas (e.g., hillslopes) filled again. A large fraction of sediment eroded from slopes therefore probably did not reach the downstream depocentre and thus the sediment delivery ratio was redefined. For our calculations we assume low sediment delivery ratios, between a conservative 15% and a more efficient 35%. We are aware that the choice of sediment delivery ratio greatly affects the final catchment denudation rate, but we proceed with these values to try to connect source and sink areas in terms of sediment budget.

4.4.3 Denudation rate

To calculate denudation rates, the sediment yield (t/ha/y) of a catchment is needed. In general there is a tendency for larger catchments to have a smaller sediment yield (Milliman and Syvitski, 1992; Syvitski et al., 2003; Verstraeten et al., 2003). However, similar to sediment delivery ratios, there is much variation with respect to catchment area and sediment yield (up to four orders of magnitude), and positive, negative and complex relationships occur (De Vente et al., 2007); thus catchment area only explains a small part of the variation in sediment transfer processes and is a poor predictor of sediment yield. De Vente et al. (2005) state that the prediction of sediment yield at catchment scale (>50 km^2) is one of the largest challenges in soil erosion research. Therefore, quantification of the sediment yield for a large catchment based on the deposited sediment volume over a long time period provides useful insight into catchment-scale sediment yield.

The sediment yield of the Tagus catchment is obtained by dividing the total sediment mass deposited in the Lower Tagus Valley and shelf sediment depocentres (3.8 x 10^{10} t) by the period of deposition (12 ky), yielding 3.2 x 10^{6} t/y. Dividing this value by the Tagus catchment area (~8 x 10^{6} ha), gives the sediment yield of ~0.4 t/ha/y (Table 2). This is a reasonable value for a catchment of this size under a natural condition (i.e., with major human influence) (Verstraeten et al., 2003), and this result suggests the approach is reasonable.

The Tagus catchment denudation rate is quantified by converting the sediment yield into a mechanical denudation rate of ~0.015 mm/y, using an average rock density of 2.7 t/m^3 (cf. Hovius, 1998). Because this number is based only on sediment *deposited* in the downstream depocentres and does not include total erosion, it should be an underestimate. To estimate the total mechanical denudation rate, the aforementioned sediment delivery ratios of 15 and 35% are used, giving a total mechanical denudation rate of 0.1 and 0.04 mm/y, respectively (Table 4). These values are in agreement with long-term (10-40 ky) erosion rates from middle European catchments, which range between 0.02 and 0.1 mm/y (Schaller et al., 2001). Also based on the sediment delivery ratios of 15 and 35%, the average Holocene sediment production in the catchment is estimated to be 1.1-2.6 t/ha/y (Table 4). These values lie on the lower end of the values obtained in large catchments over long timescales on the Iberian Peninsula (2.5-3.3 t/ha/y; Boardman and Poesen, 2006). This perhaps suggests that the lower sediment delivery ratio of 15% for the Tagus catchment for the last 12 ky is more realistic.

A calculation of erosion rate in the Spanish portion of the Tagus catchment based on sediment discharge measurements, has revealed that ~4.12 t/ha/y is currently being eroded (Rocha et al., 2005). The amount of erosion is not surprisingly much higher than our average Holocene sediment production for the whole catchment. This can be explained by the fact that the measurements from Rocha et al. (2005) reflect current erosion rates in a catchment with widespread human activities. Due to activities such as deforestation and agriculture, erosion is expected to be stronger than compared to a natural system (see Romans et al., this volume and references therein) and when compared to the average of the past 12 ky.

The sediment delivery ratio during the period from 12-7 ka was probably lower than the Holocene average, because many sediment buffers were underfilled. During the period from 7-0 ka, the sediment delivery probably increased due to filling of the buffers; this is a mechanism discussed by various authors (e.g. Covault et al., 2013; Sømme et al., 2009). Looking at our data this may be the case as well, since a low sediment delivery ratio (15%) for the 12-7 ka period and a higher sediment delivery ratio (35%) for the 7-0 ka period result in very similar sediment production values (1.4 and 1.5 t/ha/y respectively, Table 4). This exercise demonstrates the added value of a detailed knowledge of 3D depocentre distribution, size and chronology for a detailed assessment of catchment denudation through time.

5. CONCLUSIONS

The Tagus depositional system is a unique system because of the combination of a large accommodation space in the bedrock-confined Lower Tagus Valley, the steep lowstand-surface gradient (~0.60 m/km) and the narrow continental shelf (<30 km) with the Cascais and Lisbon canyons indenting the shelf break. Our model of depocentre migration on the Iberian passive margin provides a nice example for comparative studies of Quaternary source-to-sink systems worldwide.

5.1 Depocentre migration and catchment denudation

The late Quaternary Tagus depositional system is well-suited to obtain a comprehensive understanding of 3D depocentre migration of a complete fluvial-marine system since the Last Glacial Maximum. We assessed depocentre migration of the complete sediment dispersal system for the last 20 ky and adopted a time-integrated 3D reconstruction of sediment volumes in the main depocentres for the last 12 ky. We used borehole data to define depocentre architecture, and, using a multi-disciplinary and multi-proxy approach, we quantified sediment volumes and the timing of deposition. For the quantification part of this work, focus was placed on the downstream depositional areas, i.e. the Lower Tagus Valley and continental shelf where the bulk of sediments has accumulated during the last 12 ky.

From the results we conclude that:

- Between 20 and 12 ka the main depocentre was located on the Tagus Abyssal Plain, as testified by numerous turbidites (up to 10 turbidites per 500 y) and high overall sedimentation rates (1.3 mm/y);
- During the end of the glacial period the main depocentre on the Tagus Abyssal Plain was controlled by a narrow continental shelf (<30 km) which was crossed by an incised valley. Despite the fact that sea level remained ~30-70 m above the shelf break during lowstand, fluvial sediments likely bypassed the shelf via incised valleys directly funnelling into the heads of marine canyons. The narrow continental shelf was also responsible for widespread and deep incision of the fluvial network, creating ample accommodation space to be filled during the postglacial period (12-0 ka);
- Between 13.5 and 12 ka, during postglacial sea-level rise, the main depocentre was located on the continental shelf, where the sediments were deposited on top of lowstand fluvial deposits at a rate of ~2.6 mm/y;
- Due to progressive sea-level rise the main depocentre migrated landward, into the large Lower Tagus Valley, which hosts ~75% of the postglacial sediment volume;
- Since 5.5 ka, increased sediment supply and decreased sediment trapping due to decreased accommodation space in the Lower Tagus Valley depocentre led to progressive sediment export to the continental shelf depocentre, resulting in formation of a subaqueous delta with extensive prodelta. Both the Lower Tagus Valley and continental shelf depocentres experienced an increase in sediment deposition since ~2 ka caused by land-use changes in the Tagus catchment.

Our time-integrated 3D approach enabled us to identify a 2.5-fold increase in sediment storage rate after ~7 ka. This increase is hypothesized to be the combined result of climatic aridification since the end of the African Humid Period (~11.5-5.5 ka) and increased human impact during the last ~2 ky. We identified increased sediment storage during the last ~7 ky, which was not previously identified.

From our estimates, the average Holocene sediment production in the catchment (1.1-2.6 t/ha/y) and the catchment denudation rate for the last 12 ky (0.04-0.1 mm/y) are in agreement with long-term (10-40 ky) erosion rates from middle European catchments.

This study demonstrates the added value of a detailed knowledge of 3D depocentre distribution, size and chronology for a thorough assessment of catchment denudation through time. The source-to-sink approach provides a powerful tool to link deposition with erosion, to identify changes in time and to link land and ocean depocentres.

5.2 Future work

The period considered here (last ~20 ky) is ideal for detailed high-resolution studies because a large part of the sediments can still be identified, mapped and radiocarbon dated. However, for a thorough understanding of a source-to-sink system on a passive continental margin, extending the period of study to a hundred thousands of years would greatly enhance our understanding. Over such time scales sea level, climate, tectonics and sediment production have varied considerably and are likely to interact in much different ways. The lack of terrestrial data due to erosion will be the main challenge of such a study. Therefore this work should incorporate marine records and process-based catchment modelling using different sets of boundary conditions.

Contrary to a study over large time scales, investigating sediment-flux changes on small time scales would allow identification of sediment-flux variations through time which the present study does not resolve. This could reveal the progressive downstream filling of depocentres as a result of disturbances in the catchment. Sediment fluxes can possibly be related to specific climatic or historic events during the last 7 ky. Such a study would rely heavily on high-resolution radiocarbon, optically stimulated luminescence (OSL) dating and other geochronological tools.

ACKNOWLEDGEMENTS

We thank staff and students from VU University Amsterdam, Friedrich-Schiller-Universität Jena, LNEG Lisboa, IPMA and TNO. Klaas Verwer is thanked for an introduction in Petrel. Martine Hagen is thanked for core D13882 pollen analyses and Esther Bootsma for core MD03-2698 pollen analyses. We thank Sjoerd Bohncke for biogeological assistance and

Fatima Abrantes for marine geological and logistical support. We thank Tjeerd van Weering for constructive comments on an earlier draft of the manuscript. The authors also wish to thank the two anonymous reviewers and guest editor J.P. Walsh for much appreciated comments on earlier drafts of this paper. João Araújo is thanked for providing an inspiring writing environment in Portugal. This work was financed by the 01-LEC-EMA44F SEDPORT Project by the European Science Foundation under the EUROCORES Program EUROMARGINS, through contract Nr. ERAS-CT-2003-980409 of the European Commission, DG Research, FP6 and by the Division for Earth and Life Sciences (ALW) of the Netherlands Organization for Scientific Research (NWO), project 855.01.050. We thank TNO for the opportunity to publish this work.

FIGURE CAPTIONS

Figure 1. Location of study areas on the Iberian passive continental margin. The main map (a) shows the Tagus catchment and study areas on the Iberian Peninsula and the location of marine core MD03-2698. Digital elevation data from Jarvis et al. (2006), bathymetry from IOC, IHO and BODC (2003). Inset maps show (b) borehole locations in the Lower Tagus Valley and (c) borehole locations on the Tagus continental shelf. Detailed bathymetry from IPMA-DivGM (2013). The inset graphs show the topographic gradients across the subaqueous delta and shelf break (green line). The Last Glacial Maximum sea-level lowstand (-120 m relative to present-day sea level) is indicated for reference (blue line).

Figure 2. Schematic figure illustrating the study area for volumetric calculations and its relationship to other components of the depositional system.

Figure 3. Simplified 3D representation of cross sections across the Lower Tagus Valley, showing the distribution of sediments deposited below (12-7 ka, blue) and above (7-0 ka, yellow) the maximum flooding surface. The position of terrestrial core VAL (Fig. 4) is indicated on cross section Benfica do Ribatejo. Horizontal distance is not to scale. Modified after Vis et al. (2008).

Figure 4. Terrestrial core VAL illustrating the Lower Tagus Valley sedimentary fill (+7 m msl; 39°09’ N - 08°44’ W): (a) sedimentary log with calibrated radiocarbon ages (2σ); (b) grain-size distribution; and (c) average sedimentation rates.

Figure 5. Images taken from Petrel software showing 3D sediment volumes (green-red arrow points towards the north): (a) location, architecture and thickness of the three major post-12 ka depocentres; (b) morphology of the base of the valley-fill with overlying post-12 ka sediment thickness projected on that surface as colour attribute; red dots symbolize data points; (c) cross section through the downstream section of the 3D valley-fill model; colour symbolizes sediment thickness of the complete post-12 ka sediment body.

Figure 6. Isopach maps of the Tagus depositional system: (a) total sediment thickness in the Lower Tagus Valley for the period 12-0 ka; (b) thickness of sediment package deposited after 7 ka; (c) thickness of the fluvial wedge (base of reconstructed volume is the +2 m sea level surface).

Figure 7. Marine core D13882 illustrating deposits from the Tagus shelf (-87 m msl; 38°38' N - 9°27' W): (a) sedimentary log with calibrated radiocarbon ages (2σ) (*italic* ages are considered too old due to reworking); (b) grain-size distribution; (c) pollen concentration, high concentration = high sediment supply; and (d) average sedimentation rates. The sandy interval in the middle of the core is strongly winnowed. MFS = maximum flooding surface.

Figure 8. Marine core MD03-2698 from the Tagus Abyssal Plain (-4602 m msl; 38°14' N - 10°23' W): (a) sedimentary log with calibrated radiocarbon ages (2σ); (b) grain-size distribution; (c) pollen concentration, high concentration = high sediment supply; and (d) average sedimentation rates. The sandy turbidites are mineralogically similar to Lower Tagus Valley sands, suggesting their fluvial origin. In terms of morphology, this core is located on the Tagus Abyssal Plain on the levee between the Cascais Canyon in the north and the Lisbon-Setúbal canyon in the south (Lebreiro et al., 2009). See Lastras et al. (2009) for details on canyon morphology.

Figure 9. Summary figure of Tagus depocentres since ~18 ka with respect to relative sea level. The main depocentre shifted due to relative sea-level rise from the Tagus Abyssal Plain (TAP) to the Tagus shelf. Shortly after 12 ka, the landward shift to the Lower Tagus Valley (LTV) occurred and tidal, marine and fluvial sediments were deposited. The effect of winnowing on the shelf was strong when sediment supply was low (see text). After the end of rapid relative sea-level rise, the LTV progressively filled and export to the shelf started and

was amplified during the last ~2 ka by human land-use changes. MFS = maximum flooding surface, non-basal sample = not compaction-free sample, basal sample = compaction-free sample.

Figure 10. Schematic representation of Lower Tagus Valley sequence stratigraphy. Note that the lowstand system sands are not connected to the sands of the highstand system. Modified after Vis and Kasse (2009).

Figure 11. Heavy mineral composition of 11 Lower Tagus Valley samples. Samples were taken from cores and are arranged from old (left) to young (right). No large changes in heavy mineral composition are present, confirming a single upstream (fluvial) sediment source. The two oldest samples were taken from lowstand deposits and possibly suffered from long-term exposure and soil weathering, lowering the unstable mineral content. Depth relative to surface.

Table 1. Radiocarbon ages. Coordinates (X-Y) in European Datum 1950/UTM Zone 29N.

Table 2. Sediment volumes, dry bulk densities (DBD) and storage rates of the Lower Tagus Valley (LTV) and subaqueous delta. *Weighted average determined using DBD of 1.75 t/m^3 for sand, 1.4 t/m^3 for clay loam, 1.2 t/m^3 for silty clay and an estimated sand to clay loam to silty clay ratio of 0.1:0.45:0.45, based on facies distributions. ■ Weighted average determined using an estimated 0.4:0.3:0.3 sand to clay loam to silty clay ratio. ◊ Heterogeneous proximal subaqueous delta (Goodbred and Kuehl, 2000).

Table 3. Overview of sediment delivery ratios (SDR) for various catchments.

Table 4. Mechanical denudation rate and sediment production for three periods based on sediment delivery ratios (SDR) of 15 and 35%. Note that a higher sediment delivery ratio implies that less sediment has remained in the catchment, thus yielding lower values.

REFERENCES

Abrantes, F., Lebreiro, S.M., Rodrigues, T., Gil, I., Bartels-Jónsdóttir, H., Oliveira, P., Kissel, C., Grimalt, J.O., 2005. Shallow-marine sediment cores record climate variability and earthquake activity off Lisbon (Portugal) for the last 2000 years. Quat. Sci. Rev., 24: 2477–2494.

Abrantes, F., Alt-Epping, U., Lebreiro, S.M., Voelker, A., Schneider, R., 2008. Sedimentological record of tsunamis on shallow-shelf areas: The case of the 1969 AD and 1755 AD tsunamis on the Portuguese Shelf off Lisbon. Mar. Geol., 249(3-4): 283-293.
Allen, J.R.L., 1999. Geological impacts on coastal wetland landscapes: some general effects of sediment autocompaction in the Holocene of northwest Europe. Holocene, 9(1): 1-12.
Alt-Epping, U., Mil-Homens, M., Hebbeln, D., Abrantes, F., Schneider, R.R., 2007. Provenance of organic matter and nutrient conditions on a river- and upwelling influenced shelf: A case study from the Portuguese margin. Mar. Geol., 243(1-4): 169-179.
Alt-Epping, U., Stuut, J.-B.W., Hebbeln, D., Schneider, R., 2009. Variations in sediment provenance during the past 3000 years off the Tagus River, Portugal. Mar. Geol., 261(1-4): 82-91.
Alves, T.M., Gawthorpe, R.L., Hunt, D.W., Monteiro, J.H., 2003. Cenozoic tectono-sedimentary evolution of the western Iberian margin. Mar. Geol., 195(1-4): 75-108.
Azevêdo, M.T., Favaretto, S., Miola, A., Mozzi, P., Nicosia, C., Nunes, E., Sostizzo, I., 2006. Palaeoenvironments of the Tagus valley during the last 15 ka: sedimentological, palynological and micromorphological evidence of the Entre Valas SEV coring (Santarém, Portugal). Tagus Floods '06 Workshop, Abstract Book 19-21 July, 2006 Lisbon, Portugal: 68-70.
Blum, M., Martin, J., Milliken, K., Garvin, M., 2013. Paleovalley systems: Insights from Quaternary analogs and experiments. Earth Sci. Rev., 116(0): 128-169.
Blum, M.D., Törnqvist, T.E., 2000. Fluvial responses to climate and sea-level change: a review and look forward. Sedimentology, 47: 2-48.
Boardman, J., Poesen, J. (Editors), 2006. Soil erosion in Europe. John Wiley & Sons, Ltd, Chichester, 855 pp.
Brisa, 2005. A10 - Auto-estrada Bucelas/Carregado/IC3 sublanço Carregado (A1)-Benavente, travessia do Tejo no Carregado. Projecto de execução geologia e geotécnica.
Busschers, F.S., Kasse, C., van Balen, R.T., Vandenberghe, J., Cohen, K.M., Weerts, H.J.T., Wallinga, J., Johns, C., Cleveringa, P., Bunnik, F.P.M., 2007. Late Pleistocene evolution of the Rhine-Meuse system in the southern North Sea basin: imprints of climate change, sea-level oscillation and glacio-isostacy. Quat. Sci. Rev., 26(25–28): 3216-3248.
Carrión, J.S., Fuentes, N., González-Sampériz, P., Quirante, L.S., Finlayson, J.C., Fernández, S., Andrade, A., 2007. Holocene environmental change in a montane region of southern Europe with a long history of human settlement. Quat. Sci. Rev., 26(11-12): 1455-1475.
Catuneanu, O., Abreu, V., Bhattacharya, J.P., Blum, M.D., Dalrymple, R.W., Eriksson, P.G., Fielding, C.R., Fisher, W.L., Galloway, W.E., Gibling, M.R., Giles, K.A., Holbrook, J.M., Jordan, R., Kendall, C.G.S.C., Macurda, B., Martinsen, O.J., Miall, A.D., Neal, J.E., Nummedal, D., Pomar, L., Posamentier, H.W., Pratt, B.R., Sarg, J.F., Shanley, K.W., Steel, R.J., Strasser, A., Tucker, M.E., Winker, C., 2009. Towards the standardization of sequence stratigraphy. Earth Sci. Rev., 92(1–2): 1-33.
Chmura, G.L., Eisma, D., 1995. A palynological study of surface and suspended sediments on a tidal flat: implications for pollen transport and deposition in coastal waters. Mar. Geol., 128(3-4): 183-200.
Covault, J.A., Romans, B.W., Graham, S.A., Fildani, A., Hilley, G.E., 2011. Terrestrial source to deep-sea sink sediment budgets at high and low sea levels: Insights from tectonically active Southern California. Geology, 39(7): 619-622.

Covault, J.A., Craddock, W.H., Romans, B.W., Fildani, A., Gosai, M., 2013. Spatial and temporal variations in landscape evolution: historic and longer-term sediment flux through global catchments. The Journal of Geology, 121: 35-56.
Dai, D., Tan, Y., 1996. Soil erosion and sediment yield in the Upper Yangtze basin. In: D.E. Walling,B.W. Webb (Editors), Erosion and sediment yield: global and regional perspectives. IAHS Publication, pp. 191-203.
Dalrymple, R.W., Boyd, R., Zaitlin, B.A., 1994. Incised-valley systems: origin and sedimentary sequences. SEPM Special Publication, 51. Society for Sedimentary Geology, Tulsa, Oklahoma, 391 pp.
Dalrymple, R.W., 2006. Incised valleys in time and space: introduction to the volume and an explanation of the controls on valley formation and filling. In: R.W. Dalrymple, D.A. Leckie,R. Tillman (Editors), Incised valleys in time and space SEPM Special publication, pp. 5-12.
De Mendonça, A.F., 1933. Relatório das sondagens geológicas no leito do rio Tejo, entre o Beato e o Montijo. Annuário dos Serviços Hidráulicos, Imprensa Nacional 1934(1): 73-84.
De Moor, J.J.W., Verstraeten, G., 2008. Alluvial and colluvial sediment storage in the Geul River catchment (The Netherlands) - Combining field and modelling data to construct a Late Holocene sediment budget. Geomorphology, 95(3-4): 487-503.
De Stigter, H.C., Jesus, C.C., Boer, W., Richter, T.O., Costa, A., Van Weering, T.C.E., 2011. Recent sediment transport and deposition in the Lisbon–Setúbal and Cascais submarine canyons, Portuguese continental margin. Deep-Sea Research II, 58: 2321-2344.
De Vente, J., Poesen, J., Verstraeten, G., 2005. The application of semi-quantitative methods and reservoir sedimentation rates for the prediction of basin sediment yield in Spain. J. Hydrol., 305: 63-86.
De Vente, J., Poesen, J., Arabkhedri, M., Verstraeten, G., 2007. The sediment delivery problem revisited. Progress in Physical Geography, 31(2): 155-178.
DeMenocal, P., Ortiz, J., Guilderson, T., Adkins, J., Sarnthein, M., Baker, L., Yarusinsky, M., 2000. Abrupt onset and termination of the African Humid Period: rapid climate responses to gradual insolation forcing. Quat. Sci. Rev., 19(1-5): 347-361.
Erkens, G., 2009. Sediment dynamics in the Rhine catchment. Quantification of fluvial response to climate change and human impact. Ph.D. thesis Thesis, Utrecht University, Utrecht, 278 pp.
Erkens, G., Cohen, K.M., 2009. Quantification of intra-Holocene sedimentation in the Rhine-Meuse delta: A record of variable sediment delivery. In: G. Erkens (Editor), Sediment dynamics in the Rhine catchment. Quantification of fluvial response to climate change and human impact. Netherlands Geographical Studies, Utrecht, pp. 117-171.
Faegri, K., Iversen, J., 1975. Textbook of pollen analysis. Munksgaard, Copenhagen, 295 pp.
Ferro, V., Minacapilli, M., 1995. Sediment delivery processes at basin scale. Hydrological Sciences, 40(6): 703-717.
Fletcher, W.J., Boski, T., Moura, D., 2007. Palynological evidence for environmental and climatic change in the lower Guadiana valley, Portugal, during the last 13 000 years. Holocene, 17(4): 481-494.
Golosov, V.N., Ivanova, N.N., Litvin, L.F., Sidorchuk, A.Y., 1992. Sediment budgets of river catchments and river channel aggradation on the Russian plain. Geomorphology (Moscow), 4: 62-71.
Gong, S., Xiong, G., 1980. The origin and transport of sediment of the Yellow River, Proceedings of the First International Symposium on River Sedimentation, Beijing, China, pp. 43-52.

Goodbred, S.L., Kuehl, S.A., 2000. Enormous Ganges-Brahmaputra sediment discharge during strengthened early Holocene monsoon. Geology, 28(12): 1083-1086.
Hanebuth, T., Stattegger, K., Grootes, P.M., 2000. Rapid flooding of the Sunda Shelf: A late-glacial sea-level record. Science, 288(5468): 1033-1035.
Holbrook, J.M., Bhattacharya, J.P., 2012. Reappraisal of the sequence boundary in time and space: Case and considerations for an SU (subaerial unconformity) that is not a sediment bypass surface, a time barrier, or an unconformity. Earth Sci. Rev., 113(3–4): 271-302.
Hovius, N., 1998. Controls on sediment supply by large rivers. In: K.W. Shanley,P.J. McCabe (Editors), Relative Role of Eustasy, Climate, and Tectonism in Continental Rocks, SEPM Special Publication. Society for Sedimentary Geology, Tulsa.
Hughen, K.A., Baillie, M.G.L., Bard, E., Beck, J.W., Bertrand, C.J.H., Blackwell, P.G., Buck, C.E., Burr, G.S., Cutler, K.B., Damon, P.E., Edwards, R.L., Fairbanks, R.G., Friedrich, M., Guilderson, T.P., Kromer, B., McCormac, G., Manning, S., Ramsey, C.B., Reimer, P.J., Reimer, R.W., Remmele, S., Southon, J.R., Stuiver, M., Talamo, S., Taylor, F.W., van der Plicht, J., Weyhenmeyer, C.E., 2004. Marine04 marine radiocarbon age calibration, 0-26 cal kyr BP. Radiocarbon, 46(3): 1059-1086.
Ineti, 2007. INETI/LNEG Library coring database, different library entries. Instituto Geológico e Mineiro (INETI)/Laboratório Nacional de Energia e Geologia (LNEG).
Instituto-Hidrográfico-Portugal, 2008. Instituto Hidrográfico, Portugal. http://www.hidrografico.pt/.
IOC-IHO-BODC, 2003. "Centenary Edition of the GEBCO Digital Atlas", published on CD-ROM on behalf of the Intergovernmental Oceanographic Commission and the International Hydrographic Organization as part of the General Bathymetric Chart of the Oceans. In: British-Oceanographic-Data-Centre (Editor), Liverpool.
IPMA-DivGM, 2013. Bathymetry offshore Portugal. Instituto Português do Mar e da Atmosfera, Divisão de Geologia Marinha e Georecursos Marinhos, Lisbon.
Jarvis, A., Reuter, H.I., Nelson, A., Guevara, E., 2006. Hole-filled seamless SRTM data V3. International Centre for Tropical Agriculture (CIAT).
Jouanneau, J.M., Garcia, C., Oliveira, A., Rodrigues, A., Dias, J.A., Weber, O., 1998. Dispersal and deposition of suspended sediment on the shelf off the Tagus and Sado estuaries, SW Portugal. Progress in Oceanography, 42(1-4): 233-257.
Konert, M., Vandenberghe, J., 1997. Comparison of laser grain size analysis with pipette and sieve analysis: A solution for the underestimation of the clay fraction. Sedimentology, 44(3): 523-535.
Kooi, H., de Vries, J.J., 1998. Land subsidence and hydrodynamic compaction of sedimentary basins. Hydrology and Earth System Sciences, 2(2-3): 159-171.
Kuehl, S.A., Alexander, C., Harris, C., Corbett, R., Orpin, A., Walsh, J.P., others, this volume.
Lastras, G., Arzola, R.G., Masson, D.G., Wynn, R.B., Huvenne, V.A.I., Hühnerbach, V., Canals, M., 2009. Geomorphology and sedimentary features in the Central Portuguese submarine canyons, Western Iberian margin. Geomorphology, 103(3): 310-329.
Lebreiro, S., Voelker, A., Vizcaino, A., Abrantes, F., Alt-Epping, U., Jung, S., Thouveny, N., Grácia, E., 2009. Sediment instability on the Portuguese continental margin under abrupt glacial climate changes (last 60 kyr). Quat. Sci. Rev., 28: 3211-3223.
Lebreiro, S.M., 1995. Sedimentation history off Iberia: Tore seamount, Tagus and Horseshoe abyssal plains. Ph.D. Thesis, University of Cambridge, Cambridge, United Kingdom, 192 pp.
Liu, Y., Zhang, P., 1996. Erosion of material in ground surface and sediment yield in the Upper Yangtze River. International Journal of Sedimentary Research, 11: 43-53.

Lu, H., Moran, C.J., Sivapalan, M., 2005. A theoretical exploration of catchment-scale sediment delivery. Water Resour. Res., 41(W09415): 1-15.
Lusoponte, 1995. New road crossing of the Tagus in Lisbon (Main bridge geological and geotechnical study). Concessionária para a Travessia do Tejo S.A. (Ponte da Vasco Gama).
Magny, M., Miramont, C., Sivan, O., 2002. Assessment of the impact of climate and anthropogenic factors on Holocene Mediterranean vegetation in Europe on the basis of palaeohydrological records. Palaeogeography Palaeoclimatology Palaeoecology, 186(1-2): 47-59.
Masson, D.G., Arzola, R.G., Wynn, R.B., Hunt, J.E., Weaver, P.P.E., 2011. Seismic triggering of landslides and turbidity currents offshore Portugal. Geochemistry Geophysics Geosystems, 12(12): 19.
Miller, A.J., Kuehl, S.A., 2010. Shelf sedimentation on a tectonically active margin: A modern sediment budget for Poverty continental shelf, New Zealand. Mar. Geol., 270: 175-187.
Milliman, J.D., Syvitski, J.P.M., 1992. Geomorphic/Tectonic Control of Sediment Discharge to the Ocean: The Importance of Small Mountainous Rivers. The Journal of Geology, 100(5): 525-544.
Morgan, R.P.C., 2005. Soil erosion and conservation. Blackwell Publishing Ltd, 304 pp.
Mou, J., Meng, Q., 1980. Sediment delivery ratio as used in the computation of the watershed sediment yield, Beijing, China.
Mougenot, D., 1985. Progradation on the Portuguese Continental-Margin - Interpretation of Seismic Facies. Mar. Geol., 69(1-2): 113-130.
Naughton, F., Goni, M.F.S., Desprat, S., Turon, J.L., Duprat, J., Malaize, B., Joli, C., Cortijo, E., Drago, T., Freitas, M.C., 2007. Present-day and past (last 25 000 years) marine pollen signal off western Iberia. Marine Micropaleontology, 62(2): 91-114.
Nittrouer, C.A., 1999. STRATAFORM: Overview of its design and synthesis of its results. Mar. Geol., 154: 3-12.
Nittrouer, C.A., Austin, J.A., Field, M.E., Kravitz, J.H., Syvitski, J.P.M., Wiberg, P.L. (Editors), 2007. Continental Margin Sedimentation: From Sediment Transport to Sequence Stratigraphy. IAS Special Publication, 37. Blackwell Publishing, Oxford, 549 pp.
Notebaert, B., Verstraeten, G., Rommens, T., Vanmontfort, B., Govers, G., Poesen, J., 2009. Establishing a Holocene sediment budget for the river Dijle. Catena, 77(2): 150-163.
Paull, C.K., McGann, M., Sumner, E.J., Barnes, P.M., Lundsten, E.M., Anderson, K., Gwiazda, R., Edwards, B., Caress, D.W., 2014. Sub-decadal turbidite frequency during the early Holocene: Eel Fan, offshore northern California. Geology, 42(10): 955-959.
Quintela, A.C., Coutinho, M.A., Miranda, J.C., 1982. Avaliação da evolução do transporte sólido no Rio Tejo e a sua influência no leito. In: APRH (Editor), Simpósio sobre a Bacia Hidrográfica Portuguesa do Tejo. APRH, Lisbon, pp. 1-20.
Ramos, C., Reis, E., Ramos Pereira, A., Azevêdo, T.M., Nunes, E., Freitas, M.C., Andrade, C., 2002. Late Holocene evolution of the Lower Tagus alluvial plain and heavy metals content: preliminary results. Environmental Change and Water Sustainability, Instituto Pirenaico de Ecología, Zaragoza: 167-182.
Ramos, C., Reis, E., 2003. Floods in southern Portugal: their physical and human causes, impacts and human response. Mitigation and Adaptation Strategies for Global Change, 7: 267-284.
Ramos Pereira, A., Ramos, C., Reis, E., Azevêdo, T.M., Nunes, E., Freitas, M.C., Andrade, C., 2002. A dinâmica da planície aluvial do Baixo Tejo no Holocénico recente:

aplicação de métodos de análise geomorfológica e sedimentológica. Publicações da Associação Portuguesa de Geomorfólogos, APGeom, 1: 67-76.
Renssen, H., Brovkin, V., Fichefet, T., Goosse, H., 2006. Simulation of the Holocene climate evolution in Northern Africa: The termination of the African Humid Period. Quat. Int., 150: 95-102.
Richter, T.O., de Stigter, H.C., Boer, W., Jesus, C.C., van Weering, T.C.E., 2009. Dispersal of natural and anthropogenic lead through submarine canyons at the Portuguese margin. Deep-Sea Research Part I-Oceanographic Research Papers, 56(2): 267-282.
Rocha, J.S., Fernandes, J.N., Ferreira, G., 2005. Plano específico de gestão de extracção de inertes no domínio hídrico do Rio Tejo. Relatório 259/05-NRE, Laboratório Nacional de Engenharia Civil (LNEC), Departamento de Hidráulica e Ambiente, Núcleo de Recursos Hídricos e Estruturas e Ambiente, Lisboa.
Rodrigues, T., Grimalt, J.O., Abrantes, F.G., Flores, J.A., Lebreiro, S.M., 2009. Holocene interdependences of changes in sea surface temperature, productivity, and fluvial inputs in the Iberian continental shelf (Tagus mud patch). Geochemistry Geophysics Geosystems, 10.
Rodrigues, T., Grimalt, J.O., Abrantes, F., Naughton, F., Flores, J.-A., 2010. The last glacial-interglacial transition (LGIT) in the western mid-latitudes of the North Atlantic: Abrupt sea surface temperature change and sea level implications. Quat. Sci. Rev., 29(15-16): 1853-1862.
Romans, B.W., Normark, W.R., McGann, M.M., Covault, J.A., Graham, S.A., 2009. Coarse-grained sediment delivery and distribution in the Holocene Santa Monica Basin, California: Implications for evaluating source-to-sink flux at millennial time scales. Geol. Soc. Am. Bull., 121(9-10): 1394-1408.
Romans, B.W., Graham, S.A., 2013. A deep-time perspective of land-ocean linkages in the sedimentary record. Annual Review of Marine Sciences, 5: 69-94.
Schaller, M., von Blanckenburg, F., Hovius, N., Kubik, P.W., 2001. Large-scale erosion rates from in situ-produced cosmogenic nuclides in European river sediments. Earth Planet. Sci. Lett., 188(3-4): 441-458.
Shi, C.X., Zhang, D.D., You, L.Y., 2003. Sediment budget of the Yellow River delta, China: the importance of dry bulk density and implications to understanding of sediment dispersal. Mar. Geol., 199(1-2): 13-25.
Simms, A.R., Anderson, J.B., Taha, Z.P., Rodriguez, A.B., 2006. Overfilled versus underfilled incised valleys: examples from the Quaternary Gulf of Mexico. In: R.W. Dalrymple, D.A. Leckie,R. Tillman (Editors), Incised valleys in time and space. SEPM Special publication, pp. 117-139.
Sømme, T.O., Helland-Hansen, W., Martinsen, O.J., Thurmond, J.B., 2009. Relationships between morphological and sedimentological parameters in source-to-sink systems: a basis for predicting semi-quantitative characteristics in subsurface systems. Basin Res., 21(4): 361-387.
Sommerfield, C.K., Lee, H.J., 2004. Across-shelf sediment transport since the Last Glacial Maximum, southern California margin. Geology, 32(4): 345-348.
Sommerfield, C.K., Ogston, A.S., Mullenbach, B.L., Drake, D.E., Alexander, C.R., Nittrouer, C.A., Borgeld, J.C., Wheatcroft, R.A., Leithold, E.L., 2007. Oceanic Dispersal and Accumulation of River Sediment. In: C.A. Nittrouer, J.A. Austin, M.E. Field, J.H. Kravitz, J.P.M. Syvitski,P.L. Wiberg (Editors), Continental Margin Sedimentation: From Sediment Transport to Sequence Stratigraphy. Special Publication Number 37 of the International Association of Sedimentologists. Blackwell Publishing Ltd., Oxford.
Stockmarr, J., 1971. Tablets with spores used in absolute pollen analysis. Pollen et Spores, 13: 615-621.

Stuiver, M., Reimer, P.J., 1993. Extended 14C database and revised CALIB radiocarbon calibration program. Radiocarbon, 35: 215-230.
Stuiver, M., Braziunas, T.F., 1993. Modeling Atmospheric C-14 Influences and C-14 Ages of Marine Samples to 10,000 Bc. Radiocarbon, 35(1): 137-189.
Stuiver, M., Reimer, P.J., Reimer, R.W., 2005. CALIB 5.0. (internet program and documentation).
Syvitski, J.P., Morehead, M.D., 1999. Estimating river-sediment discharge to the ocean: application to the Eel margin, northern California. Mar. Geol., 154(1-4): 13-28.
Syvitski, J.P.M., Peckham, S.D., Hilberman, R., Mulder, T., 2003. Predicting the terrestrial flux of sediment to the global ocean: a planetary perspective. Sediment. Geol., 162(1-2): 5-24.
Talling, P.J., 1998. How and where do incised valleys form if sea level remains above the shelf edge? Geology, 26(1): 87-90.
Thorndycraft, V.R., Benito, G., 2006. The Holocene fluvial chronology of Spain: evidence from a newly compiled radiocarbon database. Quat. Sci. Rev., 25(3-4): 223-234.
Törnqvist, T.E., Wortman, S.R., Mateo, Z.R.P., Milne, G.A., Swenson, J.B., 2006. Did the last sea level lowstand always lead to cross-shelf valley formation and source-to-sink sediment flux? Journal of Geophysical Research-Earth Surface, 111(F4): -.
Trimble, S.W., 1983. A sediment budget for Coon Creek basin in the Driftless Area, Wisconsin, 1853-1977. Am. J. Sci., 283: 454-474.
Vale, C., Sundby, B., 1987. Suspended Sediment Fluctuations in the Tagus Estuary on Semi-Diurnal and Fortnightly Time Scales. Estuarine Coastal and Shelf Science, 25(5): 495-508.
Van Asselen, S., Stouthamer, E., Van Asch, T.W.J., 2009. Effects of peat compaction on delta evolution: A review on processes, responses, measuring and modeling. Earth Sci. Rev., 92(1-2): 35-51.
Van der Schriek, T., Passmore, D.G., Stevenson, A.C., Rolao, J., 2007. The palaeogeography of Mesolithic settlement-subsistence and shell midden formation in the Muge valley, Lower Tagus Basin, Portugal. The Holocene, 17(3): 369-385.
Van Leeuwaarden, W., Janssen, C.R., 1985. A preliminary palynological study of peat deposits near an oppidum in the Lower Tagus Valley, Portugal. Actas, Reunião do Quaternario Iberico, 2: 226-236.
Verstraeten, G., Poesen, J., de Vente, J., Koninckx, X., 2003. Sediment yield variability in Spain: a quantitative and semiqualitative analysis using reservoir sedimentation rates. Geomorphology, 50(4): 327-348.
Vis, G.-J., Kasse, C., Vandenberghe, J., 2008. Late Pleistocene and Holocene palaeogeography of the Lower Tagus Valley (Portugal): effects of relative sea level, valley morphology and sediment supply. Quat. Sci. Rev., 27(17-18): 1682-1709.
Vis, G.-J., Kasse, C., 2009. Late Quaternary valley-fill succession of the Lower Tagus Valley, Portugal. Sediment. Geol., 221: 19-39.
Vis, G.-J., Kasse, C., Kroon, D., Jung, S., Zuur, H., Prick, A., 2010a. Late Holocene sedimentary changes in floodplain and shelf environments of the Tagus River (Portugal). Proc. Geol. Assoc.
Vis, G.-J., Bohncke, S.J.P., Schneider, H., Kasse, C., Coenraads-Nederveen, S., Zuurbier, K., Rozema, J., 2010b. Holocene flooding history of the Lower Tagus Valley (Portugal). Journal of Quaternary Science, 25(8): 1222-1238.
Vis, G.-J., Cohen, K.M., Westerhoff, W.E., Ten Veen, J.H., Hijma, M.P., Van der Spek, A.J.F., Vos, P.C., 2015. Palaeogeography. In: I. Shennan, A.J. Long,B.P. Horton (Editors), Handbook of Sea-Level Research. John Wiley & Sons/American Geophysical Union, pp. 600.

Vörösmarty, C.J., Meybeck, M., Fekete, B., Sharma, K., Greena, P., Syvitski, J.P.M., 2003. Anthropogenic sediment retention: major global impact from registered river impoundments. Global and Planetary Change, 39: 169-190.
Walling, D.E., 1983. The sediment delivery problem. J. Hydrol., 65: 209-237.
Walling, D.E., 1999. Linking land use, erosion and sediment yields in river basins. Hydrobiologia, 410: 223-240.
Walling, D.E., Russell, M.A., Hodgkinson, R.A., Zhang, Y., 2002. Establishing sediment budgets for two small lowland agricultural catchments in the UK. Catena, 47: 323-353.
Walsh, J.P., Nittouer, C.A., 2009. Unerstanding fine-grained river-sediment dispersal on continental margins. Mar. Geol., 263: 34-45.
Walsh, J.P., Corbett, D.R., Ogston, A.S., Nittouer, C.A., Kuehl, S.A., Allison, M.A., Goodbred jr., S.L., 2014. Shelf and slope sedimentation associated with large deltaic systems. In: T.S. Bianchi, M.A. Allison,W.J. Cai (Editors), in Biogeochemical dynamics at major river-coastal interfaces: linkages with global change. Cambridge University Press, USA, pp. 658.
Warrick, J.A., 2014. Eel River margin source-to-sink sediment budgets: Revisited. Mar. Geol., 351: 25-37.
Weaver, P.P.E., Wynn, R.B., Kenyon, N.H., Evan, J., 2000. Continental margin sedimentation, with special reference to the north-east Atlantic margin. Sedimentology, 47: 239-256.
Weaver, P.P.E., 2003. Discovery Cruise 249, 19 Aug-10 Sep 2000. History of Sedimentation in the Gulf of Cadiz: investigations with the SOC giant piston corer, Southampton Oceanography Centre, Southampton, UK.
Wolf, D., Seim, A., Diaz del Olmo, F., Faust, D., 2013. Late Quaternary fluvial dynamics of the Jarama River in central Spain. Quat. Int., 302: 20-41.

Figure 1

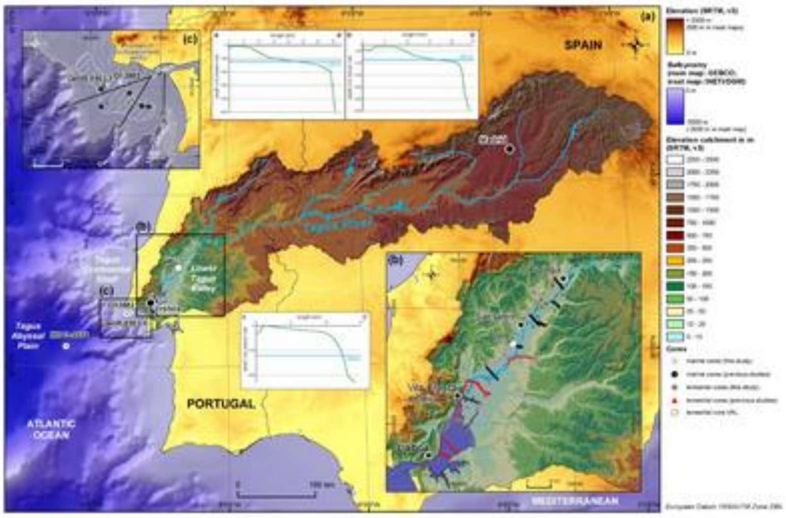

Figure 2

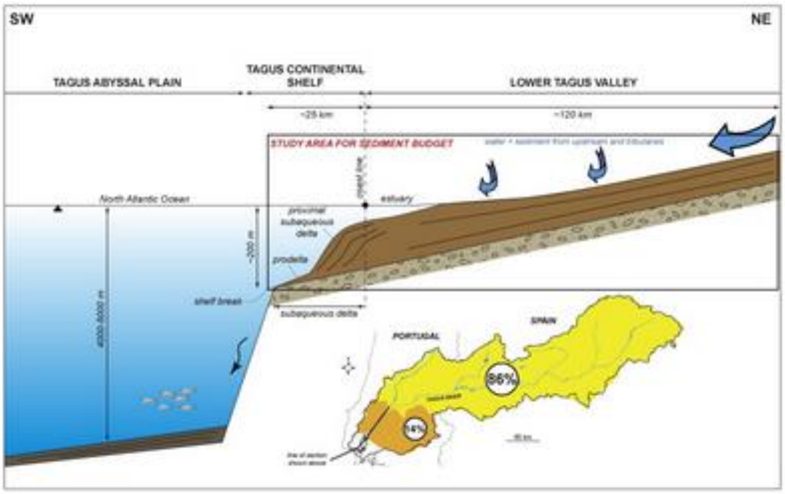

Figure 3

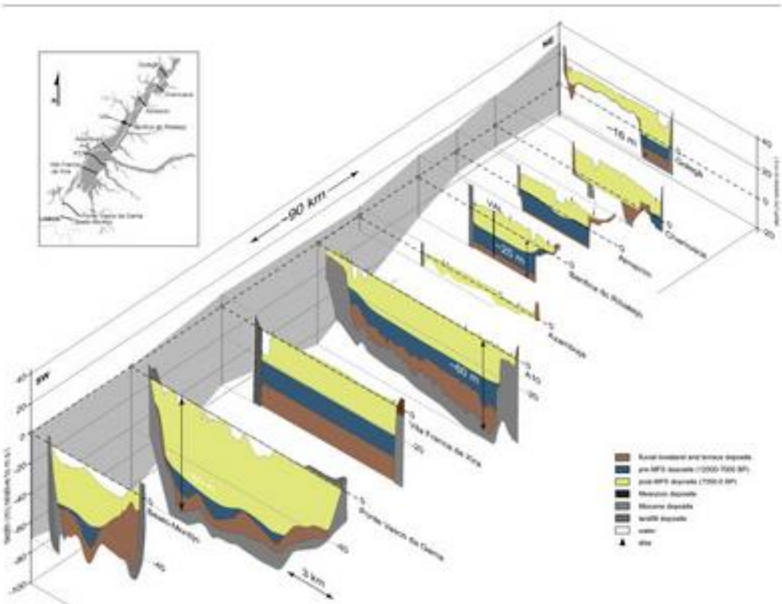

Figure 4

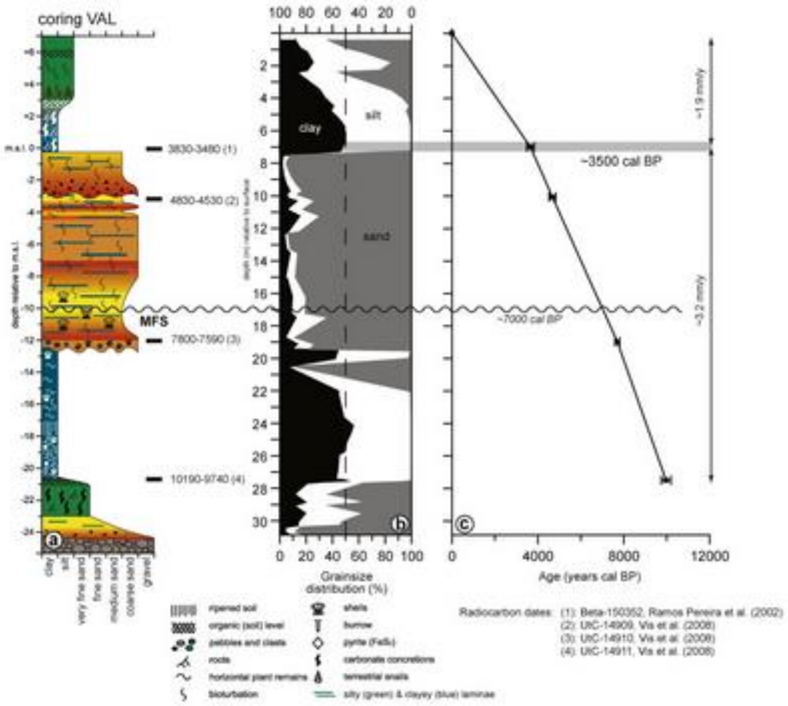

Figure 5

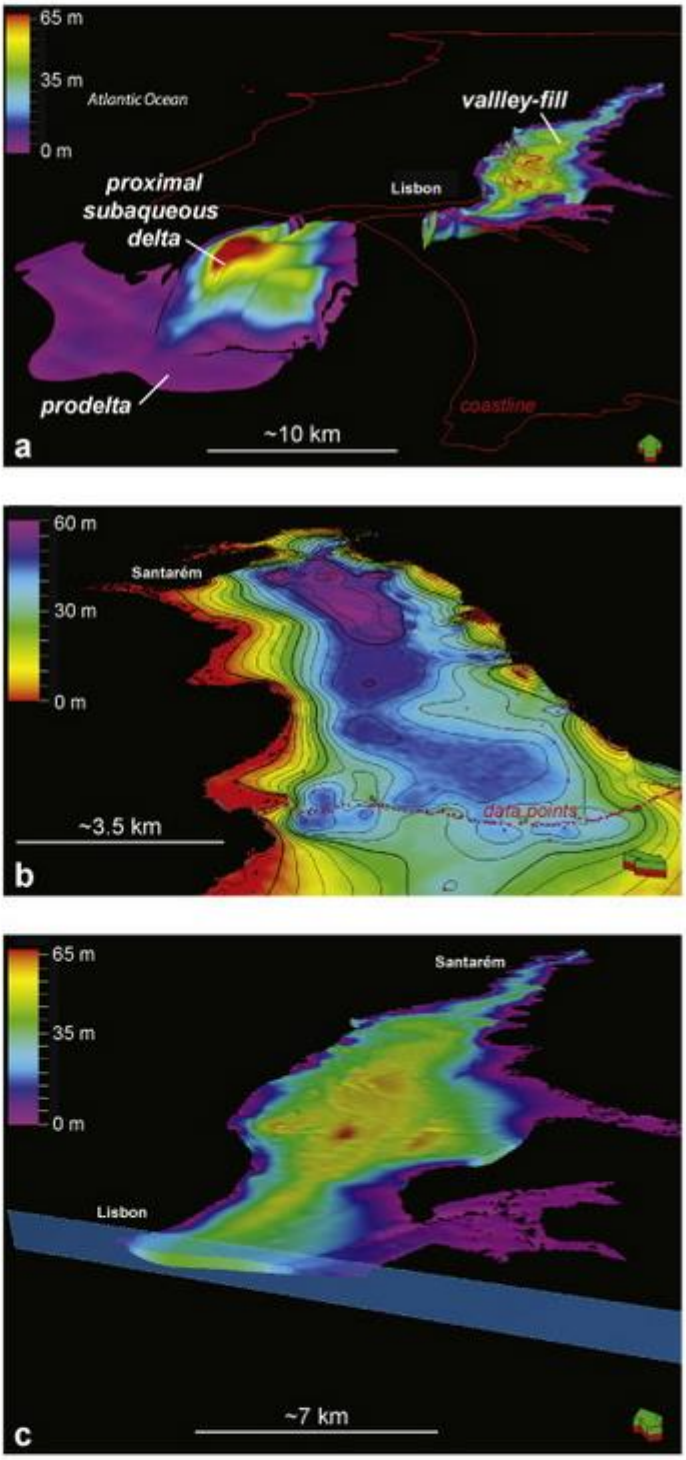
65 m
35 m
0 m
Atlantic Ocean
vallley-fill
Lisbon
proximal
subaqueous
delta
prodelta
coastline
~10 km
a
60 m
30 m
0 m
Santarém
data points
~3.5 km
b
65 m
35 m
0 m
Santarém
Lisbon
~7 km
c

Figure 6

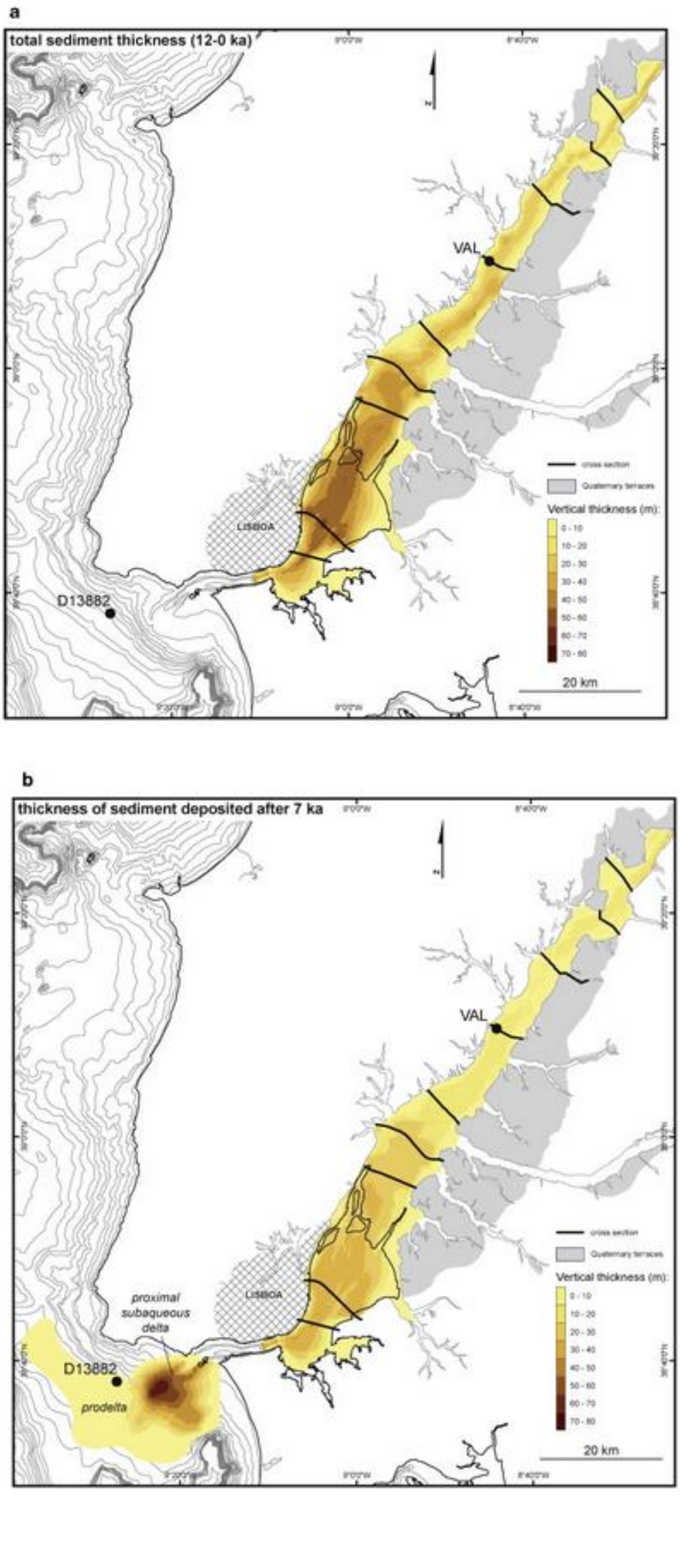
a
total sediment thickness (12-0 ka)
VAL
LISBOA
D13882
cross section
Quaternary terraces
Vertical thickness (m):
20 km
b
thickness of sediment deposited after 7 ka
VAL
LISBOA
proximal
subaqueous
delta
D13882
prodelta
cross section
Quaternary terraces
Vertical thickness (m):
20 km

c

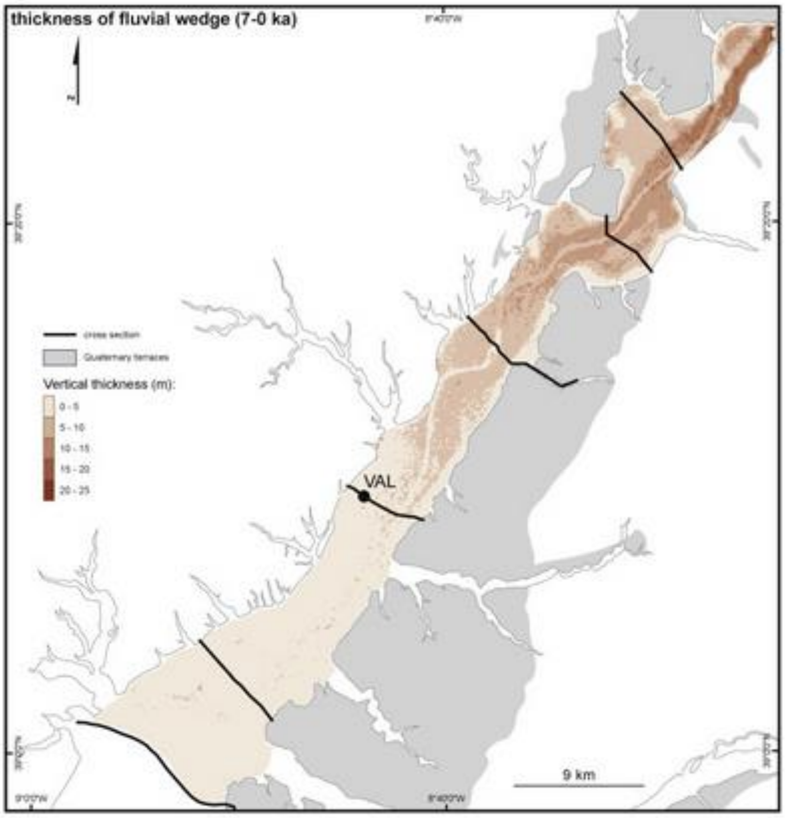
thickness of fluvial wedge (7-0 ka)
cross section
Quaternary terraces
Vertical thickness (m):
0 - 5
5 - 10
10 - 15
15 - 20
20 - 25
VAL
9 km

Figure 7

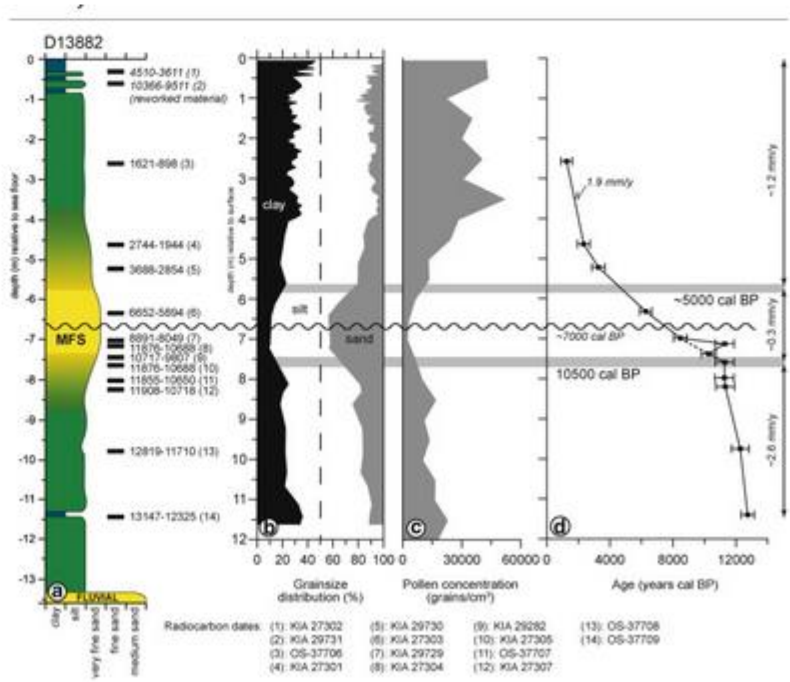
D13882
4510-3611 (1)
10366-9511 (2)
(reworked material)
1621-898 (3)
2744-1944 (4)
3688-2854 (5)
6652-5894 (6)
8891-8049 (7)
11876-10688 (8)
10717-9807 (9)
11876-10688 (10)
11855-10650 (11)
11908-10718 (12)
12819-11710 (13)
13147-12325 (14)
MFS
FLUVIAL
clay
silt
very fine sand
fine sand
medium sand
clay
silt
sand
Grainsize distribution (%)
Pollen concentration (grains/cm³)
Age (years cal BP)
1.9 mm/y
~5000 cal BP
~7000 cal BP
10500 cal BP
~1.2 mm/y
~0.3 mm/y
~2.6 mm/y
Radiocarbon dates: (1): KIA 27302
(2): KIA 29731
(3): OS-37706
(4): KIA 27301
(5): KIA 29730
(6): KIA 27303
(7): KIA 29729
(8): KIA 27304
(9): KIA 29282
(10): KIA 27305
(11): OS-37707
(12): KIA 27307
(13): OS-37708
(14): OS-37709

Figure 8

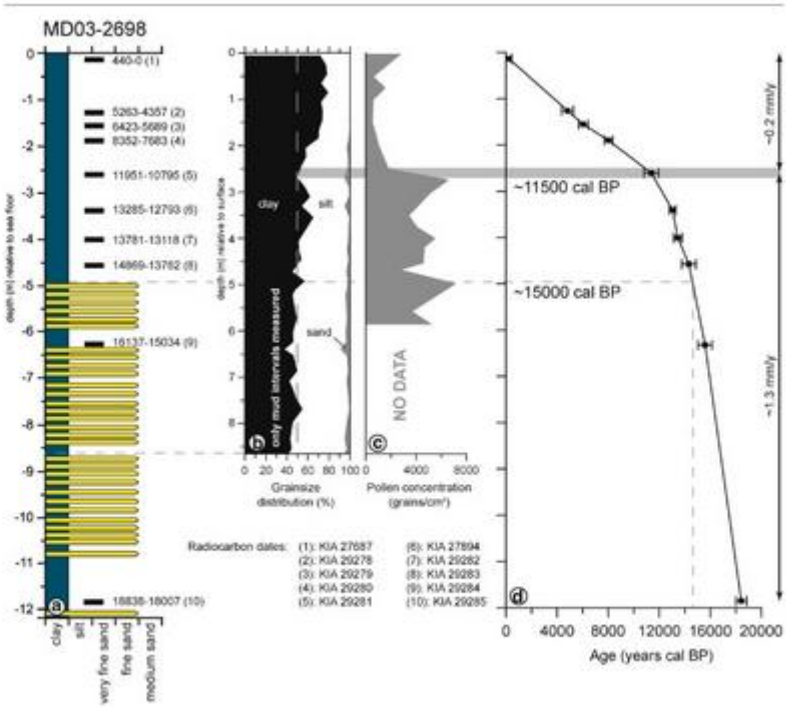

Figure 9

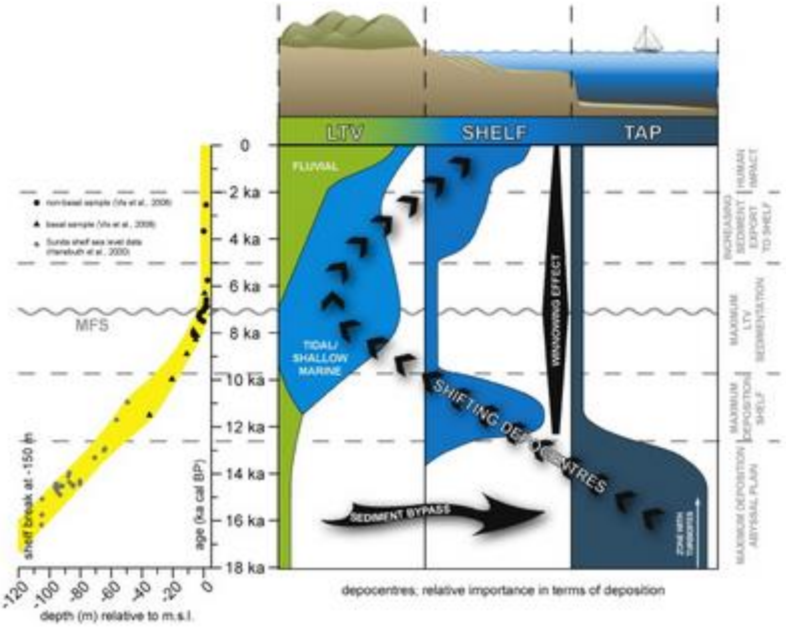

Figure 10

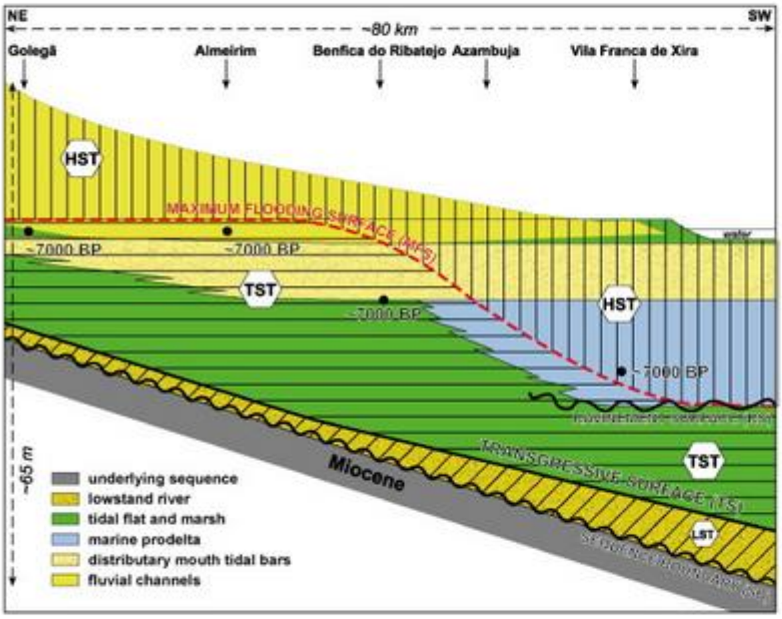

Figure 11

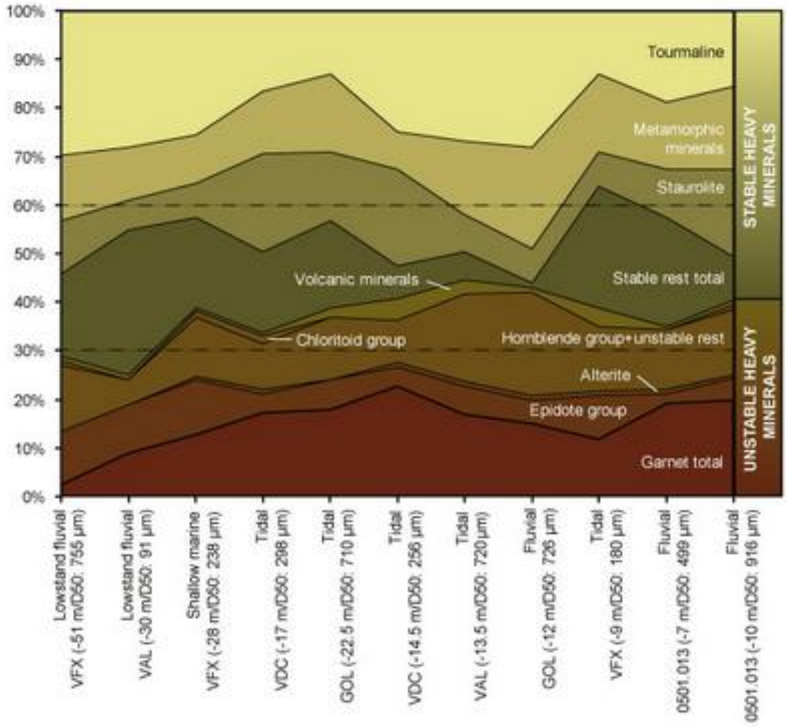

Table 1

Table 1
Radiocarbon ages. Coordinates (X-Y) in European datum 1950/UTM zone 29N.

Lab. Nr.	^{14}C age yrs. BP ± 1σ	Age cal. BP 2σ	Midpoint	Coordinates (x-y/z) (m)	Sample depth (cm)	Borehole name	Remarks	First published	Calibration curve
GrA-27234	5530 ± 45	6410–6210	6310	531812–4342025/+8	740–741	0401.003/203	–	Vis et al. (2008)	intcal04.14c
GrA-27236	2005 ± 35	2050–1870	1960	543112–4350825/+9	300–310	0401.004/204	–	Vis et al. (2008)	intcal04.14c
GrA-29205	1390 ± 35	1360–1265	1313	541501–4362494/+14.3	366–370	0401.021	Caustic extract	Vis et al. (2008)	intcal04.14c
GrA-29447	1510 ± 40	1520–1310	1415	541501–4362494/+14.3	366–370	0401.021	Residue	Vis et al. (2008)	intcal04.14c
GrA-29214	3850 ± 40	4410–4150	4280	541501–4362494/+14.3	506–508	0401.021	Caustic extract	Vis et al. (2008)	intcal04.14c
GrA-29215	3610 ± 60	4090–3720	3905	541501–4362494/+14.3	506–508	0401.021	Residue	Vis et al. (2008)	intcal04.14c
GrA-29216	4215 ± 40	4860–4610	4735	541501–4362494/+14.3	554–556	0401.021	Caustic extract	Vis et al. (2008)	intcal04.14c
GrA-29218	3945 ± 40	4520–4240	4380	541501–4362494/+14.3	554–556	0401.021	Residue	Vis et al. (2008)	intcal04.14c
GrA-29220	545 ± 35	650–510	580	544533–4358745/+16.63	370–380	0401.013	Charcoal (AAA)	Vis et al. (2008)	intcal04.14c
GrA-29221	200 ± 35	310–0	155	540649–4352679/+15.68	370–380	0401.104	Charcoal (AAA)	Vis et al. (2008)	intcal04.14c
GrA-29530	930 ± 35	930–760	845	542899–4360935/+16.23	260–270	0401.002	Sieved at 250 & 125 μm	Vis et al. (2008)	intcal04.14c
GrA-29843	65 ± 40	270–0	135	541504–4352118/+13.22	540–550	0401.015	Sieved at 250 μm	Vis et al. (2008)	intcal04.14c
GrA-29535	2490 ± 40	2730–2360	2545	541504–4352118/+13.22	840–850	0401.015	Sieved at 250 & 125 μm	Vis et al. (2008)	intcal04.14c
GrA-29538	335 ± 35	490–300	395	540649–4352679/+15.68	610–620	0401.104	Sieved at 250 μm	Vis et al. (2008)	intcal04.14c
GrA-29539	1095 ± 35	1070–930	1000	541584–4352084/+16.65	300–310	0401.106	Sieved at 250 & 125 μm	Vis et al. (2008)	intcal04.14c
GrA-30616	4485 ± 35	5300–4970	5135	542943–4350667/+12.73	923–926	0401.302/S2	Sieved at 125 μm	Vis et al. (2008)	intcal04.14c
GrA-31005	6500 ± 50	7510–7300	7405	542943–4350667/+12.73	1491–1495	0401.302/S2	Sieved at 125 μm	Vis et al. (2008)	intcal04.14c
GrA-30961	6360 ± 45	7420–7170	7295	542943–4350667/+12.73	1588–1590	0401.302/S2	Sieved at 125 μm	Vis et al. (2008)	intcal04.14c
GrA-30615	5790 ± 40	6680–6480	6580	540407–4359849/+12	1024–1029	0501.029	Sieved at 200 μm	Vis et al. (2008)	intcal04.14c
GrA-31004	5900 ± 45	6860–6630	6745	540407–4359849/+12	1046–1050	0501.029	Sieved at 200 μm	Vis et al. (2008)	intcal04.14c
GrA-30860	325 ± 30	480–300	390	548938–4364435/+25	110–120	–	Charcoal	Vis et al. (2009)	intcal04.14c
GrA-32584	8030 ± 40	9030–8750	8890	531088–4346563/+11.38	2230–2240	0501.016	Sieved at 63 μm	Vis et al. (2008)	intcal04.14c
GrA-32586	2440 ± 30	2710–2350	2530	531726–4345914/+11.07	820–830	0501.013	Sieved at 125 μm	Vis et al. (2008)	intcal04.14c
GrA-32647	2480 ± 30	2720–2360	2540	522094–4335448/+3.94	240–250	0501.042	Sieved at 125 μm	Vis et al. (2008)	intcal04.14c
GrA-33637	5640 ± 45	6510–6300	6405	522373–4335353/+4.30	1160–1170	0501.041	Sieved at 63 μm	Vis et al. (2008)	intcal04.14c
GrA-32650	600 ± 25	660–540	600	524799–4333804/+7.60	690–700	0501.030	Sieved at 125 μm	Vis et al. (2008)	intcal04.14c
GrA-32651	6165 ± 35	7170–6950	7060	526038–4333421/+7.42	770–780	0501.025	Sieved at 63 μm	Vis et al. (2008)	intcal04.14c
GrA-32654	7440 ± 40	8360–8180	8270	526038–4333421/+7.42	1260–1270	0501.025	Sieved at 63 μm	Vis et al. (2008)	intcal04.14c
GrA-32587	2625 ± 30	2785–2720	2753	514130–4322014/+4	860–880	0501.050	Sieved at 125 μm	Vis et al. (2008)	intcal04.14c
GrA-32644	450 ± 30	540–470	505	512824–4323436/+3	360–370	0501.051	Sieved at 63 μm	Vis et al. (2008)	intcal04.14c
GrA-33636	101,91 ± 0,4%	0	0	512474–4323832/+3	1590–1610	0501.052	Sieved at 63 μm	Vis et al. (2008)	intcal04.14c
GrA-32645	2555 ± 30	2760–2500	2630	514940–4321160/+4	1440–1450	0501.044	Sieved at 125 μm	Vis et al. (2008)	intcal04.14c
GrA-32646	5010 ± 35	5900–5650	5775	512474–4323832/+3	860–870	0501.052	Sieved at 63 μm	Vis et al. (2008)	intcal04.14c
GrA-32656	1765 ± 30	1820–1570	1695	504812–4310535/+2	440–480	0501.071	Sieved at 63 μm	Vis et al. (2008)	intcal04.14c
GrA-32655	6265 ± 35	7270–7020	7145	544750–4358375/+17.40	1967–1974	0401.304/S4	Sieved at 63 μm	Vis et al. (2008)	intcal04.14c
UtC-14746	2530 ± 60	2760–2360	2560	540407–4359849/+12	516–520	0501.029	Sieved at 125 μm	Vis et al. (2010b)	intcal04.14c
UtC-14747	3089 ± 38	3390–3210	3300	540407–4359849/+12	604–607	0501.029	Sieved at 125 μm	Vis et al. (2008)	intcal04.14c
UtC-14748	4129 ± 42	4830–4520	4675	540407–4359849/+12	711–712	0501.029	Sieved at 125 μm	Vis et al. (2008)	intcal04.14c
UtC-14749	1022 ± 37	1060–790	925	540407–4359849/+12	331–334	0501.029	Sieved at 125 μm	Vis et al. (2008)	intcal04.14c
UtC-14750	1136 ± 38	1180–960	1070	540407–4359849/+12	331–334	0501.029	Sieved at 125 μm	Vis et al. (2008)	intcal04.14c
UtC-14744	1630 ± 35	1610–1410	1510	526420–4333197/+5	140–150	0601.002	–	Vis et al. (2008)	intcal04.14c
UtC-14745	3849 ± 47	4420–4100	4260	526420–4333197/+5	280–290	0601.002	–	Vis et al. (2008)	intcal04.14c
UtC-14909	4145 ± 42	4830–4530	4680	523321–4334600/+7	1004–1010	0601.301	Sieved at 63 μm	Vis et al. (2008)	intcal04.14c
UtC-14910	6860 ± 50	7800–7590	7695	523321–4334600/+7	1898	0601.301	Sieved at 63 μm	Vis et al. (2008)	intcal04.14c
UtC-14911	8880 ± 60	10,190–9740	9965	523321–4334600/+7	2748–2753	0601.301	Sieved at 63 μm	Vis et al. (2008)	intcal04.14c
UtC-14904	3647 ± 41	4090–3850	3970	505439–4310324/+2	1281	0601.302	Sieved at 63 μm	Vis et al. (2008)	intcal04.14c
UtC-14905	6247 ± 46	7270–7010	7140	505439–4310324/+2	2192–2196	0601.302	Sieved at 63 μm	Vis et al. (2008)	intcal04.14c
UtC-14906	8900 ± 50	10,200–9780	9990	505439–4310324/+2	2842–2848	0601.302	Sieved at 63 μm	Vis et al. (2008)	intcal04.14c
UtC-14907	9990 ± 70	11,800–11,200	11,500	505439–4310324/+2	3710–3716	0601.302	Sieved at 63 μm	Vis et al. (2008)	intcal04.14c
UtC-14908	12,160 ± 90	14,260–13,780	14,020	505439–4310324/+2	4919–4925	0601.302	Sieved at 63 μm	Vis et al. (2008)	intcal04.14c
UtC-1983	6040 ± 50	7010–6740	6875	536620–4342720/+7.5	761–760	Alpiara III	–	Vis et al. (2010)	intcal04.14c
UtC-1984	5670 ± 40	6560–6320	6440	536620–4342720/+7.5	752–751	Alpiara III	–	Vis et al. (2010)	intcal04.14c
UtC-1985	3660 ± 40	4410–3870	4005	536620–4342720/+7.5	502–501	Alpiara III	–	Vis et al. (2010)	intcal04.14c
UtC-1986	2200 ± 40	2340–2120	2230	536620–4342720/+7.5	301–299	Alpiara III	–	Vis et al. (2010)	intcal04.14c
–	900 ± 40	?	816	530589–4347131/+11.15	103–104	SEV	–	Azevedo et al. (2006)	intcal04.14c

Table 2

	Volume (km^3)		DBD (t/m^3)		Mass (t)	Period (y)		Mean storage rate (t/y)	
12–7 ka cal BP									
LTV	6.4	×	1.35*	=	8.6×10^9	/ 5000	=	**1.7×10^6**	
								↕ ~1.7×	
7–0 ka cal BP									
LTV	*13.9*	×	*1.48* ■	=	2.1×10^{10}	/ 7000	=	*2.9×10^6*	~2.5×
Pr. sub. delta	*5.5*	×	*1.50* ◊	=	8.2×10^9	/ 7000	=	*1.2×10^6*	
Prodelta	*0.7*	×	*1.15*	=	7.8×10^8	/ 7000	=	*0.1×10^6*	
Total	20.2							**4.2×10^6**	
					Summed: 3.8×10^{10}				

↕

3.2×10^6 t/y (based on 12, 000y)

↕

0.4 t/ha/y (based on a catchment area of 8,000,000 ha, which is 80,000 km^2)

Table 3

Catchment	SDR (%)	Area (km^2)	Remark	Source
Upper Mississippi tributary (USA)	7	–		Trimble (1983)
Middle Yellow River (China)	1–100	–	High drainage density and frequent hyper-concentrated flows	Gong and Xiong, 1980; Mou and Meng, 1980; in Walling, 1999
Upper Yangtze River (China)	0.34–34	–		Dai and Tan, 1996; Liu and Zhang, 1996; in Walling, 1999
Russian Plain	0–89	–	Small- and medium-sized	Golosov et al. (1992)
agricultural (UK)	14–27	1.5–3.6	Low relief, extensive land-use and strong soil erosion	Walling et al. (2002)
Various in overview	3–90	–	SDR decreases with greater catchment size and lower average slope	Morgan (2005)
Geul (Netherlands) suspended only, last ky	7	380		De Moor and Verstraeten (2008)
Dijle (Belgium)	17	758		Notebaert et al. (2009)
Rhine (Netherlands)	low	185,000	Nearly all sediment is stored in Rhine-Meuse delta and does not reach coast	Erkens (2009)

Table 4

Period	Sediment mass (t)	SDR (%)	Mechanical denudation rate (mm/y)	Sediment production (t/ha/y)
12–0 ka	3.81×10^{10}	15	0.10	2.6
		35	0.04	1.1
12–7 ka	8.56×10^{9}	15	0.05	1.4
		35	0.02	0.6
7–0 ka	2.95×10^{10}	15	0.13	3.5
		35	0.06	1.5